Signalling Mechanisms Underlying Doxorubicin and Nox2 NADPH Oxidase-Induced Cardiomyopathy: Involvement of Mitofusin-2

McLaughlin, D., Zhao, Y., O'Neill, K. M., Edgar, K. S., Dunne, P. D., Kearney, A. M., ... McDermott, B. J. (2017). Signalling Mechanisms Underlying Doxorubicin and Nox2 NADPH Oxidase-Induced Cardiomyopathy: Involvement of Mitofusin-2. British Journal of Pharmacology. DOI: 10.1111/bph.13773

Published in:
British Journal of Pharmacology

Document Version:
Peer reviewed version

SIGNALLING MECHANISMS UNDERLYING DOXORUBICIN AND NOX2 NADPH OXIDASE-INDUCED CARDIOMYOPATHY: INVOLVEMENT OF MITOFUSIN-2

Declan McLaughlin[1], Youyou Zhao[1], Karla M. O'Neill[1], Kevin S. Edgar[1], Philip D. Dunne[2], Anna M. Kearney[1], David J. Grieve[1], Barbara J. McDermott[1]

Queen's University Belfast, [1]Wellcome-Wolfson Institute for Experimental Medicine, and [2]Centre for Cancer Research & Cell Biology, Belfast BT9 7AE, UK

Running title: Nox2/Mfn2 signalling in doxorubicin cardiotoxicity

Corresponding author: Dr David J. Grieve

Wellcome-Wolfson Institute for Experimental Medicine,

Queen's University Belfast,

97 Lisburn Road,

Belfast, BT9 7AE

UK

Tel: +44(0)2890976468

Email: d.grieve@qub.ac.uk

ABSTRACT

Background and purpose: The anthracycline doxorubicin (DOX), although successful as a first-line cancer treatment, induces cardiotoxicity linked with increased production of myocardial reactive oxygen species (ROS), with Nox2 NADPH oxidase-derived superoxide reported to play a key role. The aim of this study was to identify novel mechanisms underlying development of cardiac remodelling/dysfunction further to DOX-stimulated Nox2 activation.

Experimental approach: $Nox2^{-/-}$ and wild-type (WT) littermate mice were administered DOX (12mg/kg over 3 weeks) prior to study at 4 weeks. Detailed mechanisms were investigated in murine HL-1 cardiomyocytes, employing a robust model of oxidative stress, gene silencing and pharmacological tools.

Key results: DOX-induced cardiac dysfunction, cardiomyocyte remodelling, superoxide production and apoptosis in WT mice were attenuated in $Nox2^{-/-}$ mice. Transcriptional analysis of LV tissue identified 152 differentially-regulated genes (using adjusted $P<0.1$) in DOX-treated $Nox2^{-/-}$ versus WT mice and network analysis highlighted 'Cell death and survival' as the biological function most significant to the dataset. The mitochondrial membrane protein, mitofusin-2 (Mfn2), appeared as a strong candidate, with increased expression (1.5-fold), confirmed by qPCR (1.3-fold), matching clear published evidence of promotion of cardiomyocyte cell death. In HL-1 cardiomyocytes, targeted siRNA knockdown of Nox2 decreased Mfn2 protein expression, but not vice versa. While inhibition of Nox2 activity along with DOX treatment attenuated its apoptotic and cytotoxic effects, reduced apoptosis after Mfn2 silencing reflected a sustained cytotoxic response and reduced cell viability.

Conclusions and implications: DOX-induced and Nox2-mediated upregulation of Mfn2, rather than contributing to cardiomyocyte dysfunction through apoptotic pathways, appears to promote a protective mechanism.

ABBREVIATIONS

AFC, glycyl-phenylalanyl-aminofluorocoumarin; DOX, doxorubicin; DPI, diphenyleneiodonium; HPRT, hypoxanthine phosphoribosyltransferase; HSP, heat shock protein; IVSD, interventricular septal thickness in systole; IVSS, left ventricular posterior wall dimension in diastole; LF2000, Lipofectamine™ 2000; L-NAME, L-N^G-nitroarginine methyl ester; LV, left ventricular; LVEDD, left ventricular end-diastolic diameter; LVPWD, left ventricular posterior wall dimension in diastole; LVPWS, left ventricular posterior wall dimension in systole; LVESD, left ventricular end-systolic diameter; Mfn2, mitofusin-2; MMP, matrix metalloproteinase; MTT, 3-(4, 5-dimethylthiazol-2-yl)-2, 5-diphenyltetrazolium; MV, mitral valve; PARP-1, poly ADP ribose polymerase-1; PBMCs, peripheral blood mononuclear cells; PDK1, 3-phosphoinositide dependent protein kinase 1; PGC-1α, peroxisome activated receptor gamma coactivator-1α; R110, bis-alanylalanyl-phenylalanyl-rhodamine 110; ROS, reactive oxygen species; siRNA, short-interfering RNA; WT, wild-type.

INTRODUCTION

Anthracycline drugs, such as doxorubicin (DOX), are effective anti-tumour drugs commonly prescribed to treat haematological malignancies and solid tumours, but their use is severely limited by a dose-dependent, cumulative and irrevocable cardiotoxicity. This is characterised by significant changes in cardiomyocyte biology and the extracellular matrix – the process of cardiac remodelling, which progresses to chamber dilatation, contractile dysfunction and chronic heart failure (Bloom *et al*., 2016). Current therapeutic strategies for DOX cardiotoxicity include standard heart failure medications, such as β-adrenoceptor antagonists, angiotensin receptor antagonists and angiotensin converting enzyme inhibitors, which can reduce the progression of early cardiotoxicity, although their efficacy in the longer term is limited (Cardinale *et al*., 2015; Spallarossa *et al*., 2016). Use of cardioprotective agents, such as desrazoxane, has shown benefits in certain patient groupings and so modulation of redox mechanisms is considered a worthwhile tactic, although how to target these is not at all clear (Deidda *et al*., 2015). Thus, further understanding of the molecular phenotype and signalling mechanisms of DOX-induced cardiotoxicity is fundamental to development of effective preventive strategies, and thereby improved chemotherapy outcome.

Cardiomyocyte loss through cell death pathways is a customary paradigm to explain functional deficit in the heart and there is ample experimental evidence to support DOX-induced apoptosis, necrosis and autophagy, as reviewed by Carvalho *et al*. (2014). One of the major tenets of the action of DOX is based on its interference with iron metabolism and generation of excess of reactive oxygen species (ROS). However, although antioxidants, such as co-enzyme Q10, N-acetylcysteine and vitamins C and E, have been reported to exert cardioprotective effects in experimental models (Sterba *et al*., 2013), results of small randomised clinical trials have not shown clear benefit (van Dalen *et al*., 2011; Vincent *et al*., 2013). The lack of success of antioxidant therapeutic strategies is likely to demonstrate the complexity of redox reactions in biological tissues (Madamanchi and Runge, 2013), in which ROS are known to serve both physiological and maladaptive roles. It is likely, therefore, that selective targeting of particular sources of ROS or downstream effectors may represent a more viable approach. In addition to NOS signalling, ROS generated through NADPH oxidase play an essential role in cardiac pathophysiology, regulating major elements of cardiac remodelling, such as fibrosis and apoptosis (Grieve *et al*., 2006; Gilleron *et al*., 2009). There is accumulating evidence to support an important role for Nox2 NADPH oxidase in DOX-induced cardiotoxicity, identified using Nox2-deficient ($Nox2^{-/-}$) mice (Wojnowski *et al*., 2005; Deng *et al*., 2007; Zhao *et al*., 2010).

Indeed, our group previously reported that DOX-induced interstitial fibrosis, leukocyte infiltration, cardiomyocyte apoptosis and atrophy, and cardiac dysfunction were attenuated in Nox2$^{-/-}$ mice (Zhao *et al*., 2010).

A great deal of mechanistic work has been performed in both *in vivo* and *in vitro* models from which a complex picture of signalling pathways underlying DOX-induced cardiotoxicity has emerged, in which cell death is balanced by intracellular survival signalling, linked to neuregulin / ErbB2 and Akt activation (Ghigo *et al*., 2106). In promoting cell death, oxidative stress from ROS, including superoxide and peroxynitrite, cause activation of kinase pathways (MAPK kinase 4/7, checkpoint kinase 2, stress-activated protein kinase, c-Jun N-terminal kinase). Suppression of transcription factors, GATA-4 (Kobayashi *et al*., 2006; Suzuki, 2011) and p300 (Poizat *et al*., 2005), is also linked to regulation of cell survival. Induction of small heat shock proteins (e.g. HSP20, HSP21, HSP2, HSP70) can be either cardioprotective or detrimental in this setting (Liu *et al*., 2007; Vedam *et al*., 2010; Wang *et al*., 2016). Other putative mechanisms include damage to nuclear DNA, disruption of sarcomeric protein synthesis (Ito *et al*., 1990), accumulation of the tumour suppressor protein, p53 (Yoshida *et al*., 2009) and disturbance of energy metabolism (Tokarska-Schlattner *et al*., 2006). In mitochondria, increased ROS leads to Ca^{2+} overload which triggers mitochondrial permeability transition, resulting in loss of membrane potential, swelling and outer membrane rupture, and consequent activation of caspases, release of cytochrome *c* and apoptosis.

Considering the strong evidence supporting a key role for Nox2-derived ROS in DOX-induced cardiotoxicity and the large number of possible signalling pathways identified, the primary purpose of this investigation was to highlight relevant Nox2-regulated genes and potential networks in this setting. Use of mRNA microarray technology (Kuhn *et al*. 2004) and the Nox2$^{-/-}$ mouse model (Zhao *et al*., 2010) was considered a suitable approach. Having identified the mitochondrial membrane protein, mitofusin-2 (Mfn2), as a strong candidate, the hypothesis that upregulated Mfn2 contributes to cardiomyocyte death processes induced by DOX was tested.

MATERIALS AND METHODS

Experimental Model

Animals: Mouse models incorporating genetic disruption underpin mechanistic evaluation of the contribution of particularly signalling pathways, and here we have used Nox2$^{-/-}$ mice to investigate the influence of ROS production and downstream effectors in DOX-induced cardiotoxicity. Nox2$^{-/-}$ mice on a C57BL/6J background (Pollock *et al*., 1995), originally

obtained from Jackson Laboratories (Bar Harbor, USA), were bred from an established colony at Queen's University Belfast. The principles set out in the Animal Research Reporting *In Vivo* Experiments (ARRIVE) and BJP guidelines on reporting experiments involving animals (Curtis *et al*., 2015; McGrath & Lilley, 2015) were considered throughout the study. All experimental procedures were carried out in accordance with the Home Office *Guidance on the Operation of the Animals (Scientific Procedures) Act 1986*, published by Her Majesty's Stationary Office, London, and approved by the Queen's University Belfast Animal Welfare and Ethical Review Body (PPL2714). All mice were housed in the Queen's University Belfast Biological Services Unit under controlled conditions (12h light-dark cycle, 21 °C) in standard caging, typically together with 3-5 littermates.

DOX administration: Male Nox2$^{-/-}$ and wild-type (WT) littermate controls (8-10 weeks old, 25-28g) were randomised prior to light anaesthesia with 1.5% isofluorane for administration of a cumulative dose of 12mg/kg DOX or saline control by 3 weekly injections (4mg/kg i.p. at 0, 7 and 14 days). All subsequent analyses were performed 4 weeks after the first injection. Selection of the 4 week time point was based on the progression of DOX-induced cardiac contractile dysfunction by which time a maximum decrease in percentage fractional shortening was achieved (Figure S1).

Assessment of cardiac remodelling

Echocardiography: Mice were anaesthetised with 1.5% isofluorane/oxygen, placed on a warming pad and imaged in the supine position using a Vevo770® ultrasound system with high-frequency 45MHz RMV707B scan head (VisualSonics Inc.). M-mode parasternal short-axis scans at the level of the papillary muscles were used to quantify LV wall thickness (interventricular septal thickness in diastole, IVSD; interventricular septal thickness in systole, IVSS; left ventricular posterior wall dimension in diastole, LVPWD; left ventricular posterior wall dimension in systole, LVPWS) and LV end-diastolic and end-systolic diameters (LVEDD, LVESD) from which percentage fractional shortening was calculated (LVEDD-LVESD)/LVEDD*100). Pulse-wave Doppler was used to quantify mitral valve (MV) flow, expressed as E/A ratio.

Morphometric assessment: Deep anaesthesia was induced by injection of sodium pentobarbitone (Euthanal®; 200mg/kg, i.p.) before the heart was excised and ventricles divided. Left ventricular (LV) weight was taken and indexed to tibial length. LV tissue was cut into transverse sections, which were flash frozen in liquid nitrogen prior to storage at -80°C or immersed in 10% (v/v) neutral-buffered formalin for histological analyses.

Histological analyses: Fixed LV tissue was dehydrated using graded ethanol solutions (30-100%, v/v) and xylene, before embedding in paraffin wax and cutting of thin sections (5µm). Standard haematoxylin and eosin staining was used to quantify cardiomyocyte cross-sectional area, analysing only cells with centrally located nuclei. Cardiomyocyte apoptosis was assessed by TUNEL staining (Roche Diagnostics). TUNEL-positive nuclei were expressed as % total nuclei stained with DAPI (1:1000; Invitrogen) in the same sections. For analysis of both cardiomyocyte cross-sectional area and TUNEL staining, LV sections were visualised by fluorescence microscopy and quantified using blinded digital image analysis (NIS-Elements). Each slide contained at least four sections, which were each divided into four microscopic areas, from which five separate cells were measured, such that for one animal, a total of 80 cells was analysed.

NADPH oxidase activity

LV tissue samples stored at -80°C were homogenised in lysis buffer (20mM HEPES, 4mM EGTA, 1mM DTT, 6.25µl/ml protease inhibitor cocktail; 1ml/100mg), sonicated and membrane fractions prepared from supernatants by centrifugation at 12000g for 60min. In samples diluted to a concentration of 1mg protein/ml, NADPH-dependent superoxide production was measured by lucigenin (5µM)-enhanced chemiluminescence at 37°C for 30min (Zhao *et al*., 2010). Potential sources of superoxide were assessed in experiments including: (a) tiron (20mM), cell-permeable superoxide scavenger; (b) diphenyleneiodonium (DPI, 10µM), inhibitor of NADPH oxidase and other flavoproteins; (c) L-N^G-nitroarginine methyl ester (L-NAME, 1mM), inhibitor of superoxide production by dysfunctional NOS; (d) oxypurinol (100µM), xanthine oxidase inhibitor and (e) rotenone (10µM), which inhibits the mitochondrial electron transport chain.

Gene expression analysis using real-time RT-PCR

Total RNA was extracted from LV homogenate using TRI-Reagent (Sigma-Aldrich). RNA concentration was measured at 260nm using a Thermo Scientific NanoDrop™ 1000 spectrophotometer and purity determined as the 260:280nm ratio: samples with readings 1.8-2.0 were considered of acceptable purity and taken forward at equal concentrations for reverse transcription using a High Capacity cDNA Reverse Transcription Kit (Applied Biosystems). Quantification of mRNA expression was performed by real-time RT-PCR using Power SYBR®Green on an ABI 7300 Real Time PCR System (Applied Biosystems) using standard procedures. Primer Express Software (Applied Biosystems) was used to generate mouse-specific primer pairs (Table S1), which were custom synthesised by Invitrogen. Pre-designed

and validated inventoried TaqMan® Gene Expression Assays with a FAM™ labelled probe (Applied Biosystems) were also employed for quantification of Nox2 mRNA expression. Difference in threshold cycle (Ct) for a particular PCR product from that of an endogenous control, β-actin (ΔCt), was calculated and data were expressed in each experiment relative to the control group (ΔΔCt).

Western blotting

LV protein was extracted by homogenisation with ice-cold RIPA buffer, as previously described (Zhao *et al*., 2010) and 20µg loaded onto a 10% SDS-PAGE gel before blotting on a polyvinylidene fluoride membrane (Immobilon-FL; Millipore). Membranes were incubated overnight at 4°C with a rabbit monoclonal antibody against Nox2 (1:1000, Abcam ab129068) using hypoxanthine phosphoribosyltransferase (HPRT) antibody (1:10,000, ab109021 Abcam) as a loading control. This was followed by incubation with horseradish peroxidase-labelled goat anti-rabbit secondary antibody (1:10,000 Cell Signaling Technology #7074P2) for 60min at room temperature, before the membrane was developed in a darkroom using Immobilon Western Chemiluminescent HRP Substrate (Millipore), scanned and quantified by densitometry (ImageJ). Variations in band density were expressed as fold changes compared with the HPRT control.

Gene expression profiling

LV tissue was obtained from three male Nox2$^{-/-}$ and three WT littermate controls, treated with DOX, as above. Prior to sacrifice at 4 weeks, contractile dysfunction was confirmed in WT but not Nox2$^{-/-}$ mice, demonstrating that these animals developed a similar cardiotoxicity to those in the experimental cohorts. LV tissue was homogenised, total RNA extracted and quantitative/qualitative analyses were performed as above to check adequate purity and then diluted to a pre-determined concentration of 100ng/µl of RNA in 20µl diethylpyrocarbonate-treated water. Microarray analysis including quality control assessment was conducted by Cambridge Genomics Services.

Quality control: Initially, the RNA Integrity Number for all gene array samples was shown to have a ratio of 2:1, confirming that no significant degradation of RNA product had occurred. RNA samples were amplified using the Ambion Illumina® TotalPrep RNA Amplification Kit, incorporating biotin for hybridisation with an Illumina MouseWG-6 v2.0 array. After hybridisation, the bead array was washed, stained and scanned (Illumina Iscan) and files were loaded into Genome Studio (Illumina) to assess performance of the analysis with the following

checks included: (a) hybridisation - three concentrations of Cy3-labeled oligonucleotides, each with perfect matches to control probes on the bead array; (b) low stringency - two sample independent oligonucleotides, a mismatch (mm2) probe and a perfect match (pm) probe, both compared to a control oligonucleotide; (c) high stringency - one probe corresponding to a Cy3-labeled oligonucleotide target, probe-target pairing having a high GC base pair content; (d) biotin staining - a sample-independent specific labelled oligonucleotide matched and bound to a probe on the microarray, (e) background - oligonucleotides of a random sequence, selected to have no corresponding targets in the genome, the mean signal of these oligonucleotide-probe interactions representing the imaging system background as well as any signal resulting from non-specific binding of dye or cross-hybridisation; (f) signal intensity - housekeeping genes and 'all gene' controls (Illumina) to check for sample degradation, including two oligonucleotides per gene matched with targets on the bead array.

To assess biological correlation within and between experimental groups, data were exported to the software package *R* and analysed using the embedded *lumi* package from Bioconductor (Du *et al*., 2008). Data were initially filtered to remove any probes not detected at least once in the array readout. Values close to background were also deleted to prevent these genes adding noise to the data. A threshold for selection was set at $P<0.01$ and this criterion was applied in such a way that for a gene to be detected, it had to be present in all the samples. The new data set was then re-analysed employing less stringent parameters, whereby genes were selected based on the presence on at least one of the arrays or samples analysed. Probes that met these criteria were transformed using a variance stabilisation algorithm (Lin *et al*., 2008), similar to a log2 transformation, prior to quantile normalisation. Using correlation analysis, samples were plotted against each other, such that those with a high correlation value (close to 1) show similar expression profiles, while those with a high negative correlation value (i.e. close to -1) show different expression profiles. As the aim of this study was to highlight and subsequently validate the biologically-relevant signalling pathways underpinning differential DOX-induced cardiac remodelling in WT vs $Nox2^{-/-}$ mice, an established holistic pathway approach using low stringency selection of genes of interest was followed. This prevents exclusion of potentially important gene changes which may become more relevant when viewed in the context of altered expression of an entire signalling pathway (see below).

Hierarchical clustering of samples and principal component analysis were performed in our laboratory using Partek Genomics Suite with default parameters. Data matrices were standardised to the median value of probe sets expression. Standardisation of the data allows

for comparison of expression levels for different probe sets. Following standardisation, 2-dimensional hierarchical clustering was performed (samples x probe sets/genes). Euclidean distance was used to calculate the distance matrix, a multidimensional matrix representing the distance from each data point (probe set-sample pair) to all the other data points. Ward's linkage method was subsequently applied to join samples and genes together, with the minimum variance, to find compact clusters based on the calculated distance matrix.

Identification of genes differentially expressed in WT versus Nox2$^{-/-}$ hearts: The normalised data set was analysed using the *limma* package from Bioconductor to generate LogFC (log_2 fold change) values for each probe (gene ID), each with an associated P value from application of a modified t-test. The False Discovery Rate adjusted P value, controlling for the number of false positives in tests that produce a significant result, was used as the primary filtering parameter.

Network analysis: In order to identify potential signalling pathways regulated by differentially expressed genes, Ingenuity Pathway Analysis software incorporating the Ingenuity Knowledge Base, curated from primary literature, as well as public and third-party databases, was used to analyse the normalised dataset. An adjusted P value of <0.1 was applied to include a sufficient number of genes for generation of candidate molecules and pathways.

Gene expression by real-time RT-PCR: mRNA analysis of the most relevant genes was performed in LV tissue from all experimental groups, and primer sequences are shown in Table S1.

HL-1 cardiomyocyte model

HL-1 cardiomyocytes were a gift from Dr. William C. Claycomb (Louisiana State University Health Science Centre, New Orleans). Cells were grown in T75 flasks coated with gelatin (0.02%) plus fibronectin (12.5mg/ml) and were maintained in Claycomb medium (Sigma-Aldrich), supplemented with 10% FBS, 2mM L-glutamine, 10mM penicillin–streptomycin (Life Technologies) and 10mM norepinephrine (Sigma-Aldrich) at 37°C and 5% CO_2. The culture medium was changed approximately every 48h and cells were passaged upon reaching 80-90% confluency.

Acute DOX stimulation of HL-1 cardiomyocytes: For different experiments**,** cells were seeded in 12 or 24 or 96 well plates (Nunc) at a density of 400,000 or 200,000 or 100,000 cells/well, respectively. After 24h, cells were washed with PBS to remove cellular debris and

then treated with normal supplemented Claycomb medium (as above) as a control or with DOX (0.5, 5.0 or 50µM) for 3 or 6h.

Characterisation of HL-1 model (protein expression, ROS production): For Western blotting, cell extracts were prepared by addition of ice cold RIPA buffer (300µl per well of a 12 well plate; 1ml per T25 or T75 cell culture flask) containing protease inhibitor cocktail (200µl/40ml). Cells were scraped from the adherent layer, the cell suspension was centrifuged at 12000g for 15-20min at 4°C and the supernatant analysed for protein before Western analysis was performed as described above using primary antibodies detecting Nox2 (1:1000, Abcam ab129068) and Mfn2 (1:1000 Abcam ab50838). For measurement of ROS production, homogenates were prepared by probe sonication of the whole cell preparation on ice for 20 seconds and lucigenin-enhanced chemiluminescence determined as above.

Transfection of HL-1 cardiomyocytes

HL-1 cardiomyocytes were plated on the day before transfection in the absence of norepinephrine or antibiotic. Cells were then transfected using (1) Lipofectamine™ 2000 (LF2000, Life Technologies) with Silencer Select® short-interfering RNAs (siRNAs; Ambion, Life Technologies) against Mfn2 (4390771-s100687) or Nox2 (4390771-s64650), together with a Universal Negative Control (4390844), or (2) Dharmafect 1 Transfection Reagent (Dharmacon) along with SMARTpool ON-TARGETplus siRNA against Mfn2 (L-046303-00-0005) or Nox2 (L-058659-00-000), both according to the manufacturer's instructions and following a Claycomb modified protocol. Briefly, for each well of a 24 well plate, LF2000 (5µl) was diluted in DMEM (100µl) without serum or antibiotics and incubated for 5min at room temperature. To this was added siRNA (200pM) in DMEM (100µl) followed by incubation for 20min before addition of norepinephrine/antibiotic-free Claycomb medium containing 12.5% serum (0.8ml). Culture medium was removed from each well, replaced with transfection medium and incubated at 37°C in a humidified CO_2 incubator for 18h, at which time a further 1ml of norepinephrine/antibiotic-free media was added. After 24h, transfection medium was replaced with norepinephrine-free supplemented Claycomb medium, without or with DOX as detailed in experiments below. Knockdown of targeted genes was quantified using Western blotting methods as previously outlined.

Measurement of cell death processes in HL-1 cardiomyocytes

The ApoTox-Glo™ Triplex assay (Promega) combines assessment of cell viability, cytotoxicity and caspase activation events within a single assay well. The first step simultaneously measures

live and dead-cell protease activities, using the fluorogenic substrates, glycyl-phenylalanyl-aminofluorocoumarin (AFC) and bis-alanylalanyl-phenylalanyl-rhodamine 110 (R110), respectively. In the subsequent step utilising the Caspase-Glo® Assay Technology, a caspase-3/7 substrate (tetrapeptide sequence DEVD) is added in a reagent optimised for caspase activity and generation of a luminescent signal produced by luciferase.

After treatments under control conditions or with DOX (5µM) for 24h, with or without pre-exposure to transfection or siRNA agents, the AFC/R110 reagent (100µl) was added to each well of a 24 well plate, in parallel with no cell control wells. The plate was wrapped in aluminium foil and incubated at 37°C for 90min. Fluorescence was measured using a TECAN Safire plate reader at excitation/emission wavelengths of 400/505nm and 480/520nm for measurement of AFC and R110, respectively. Then caspase 3/7 substrate (50µl) was added to the wells and the plate incubated at room temperature for 1h. The solution in each well was mixed and the cell suspension decanted in 50µl amounts, in quadruplicate, into black, opaque-walled 96 well plates and luminescence measured using a Berthold Tristar LB941 Multimode Reader luminometer. In all cases, background was accounted for by subtraction of the no cell control readings.

In a second set of experiments, HL1 cells were cultured in norepinephrine/antibiotic-free medium for 24h prior to being reverse transfected to deplete Mfn2 and then seeded onto a 96 well plate using Dharmafect 1 and 100nM ON-TARGET plus SMARTpool Mfn2 siRNA or a matched concentration of non-targeting siRNA (GE Healthcare Dharmacon Inc.). Medium was replaced with fresh complete media (containing norepinephrine but no antibiotics) 24h post-transfection. Cells were then treated with DOX (3µM) 48h post-transfection (for 24h). Endpoint measurements included caspase 3/7 activity (Caspase-Glo® 3/7 Assay, Promega) performed according to manufacturer's instructions and cell viability assessed in each condition using 3-(4, 5-dimethylthiazol-2-yl)-2, 5-diphenyltetrazolium (MTT, 0.5g/L). After removal of medium, DMSO (100µl) was added to each well, incubated at 37°C for 15min and absorbance read at 570nm. An additional readout of caspase-3 mediated apoptosis was obtained by assessing cleaved poly ADP ribose polymerase 1 (PARP-1) using a Pierce Colorimetric In-Cell ELISA Kit (Thermo Fisher) supplied with a whole-cell stain (Janus Green).

Inhibition of NADPH oxidase using VAS2870

HL-1 cardiomyocytes in 24 well plates were pre-treated with the pan-NADPH oxidase inhibitor, VAS2870 (10, 50 and 100µM in 500µl fresh culture medium), for 30min. A further 500µl culture medium containing 10µM DOX and the inhibitor was added to each well, giving

a final concentration of DOX of 5µM. Cells were incubated for 24h at 37ºC prior to ApoTox-Glo™ Triplex assay as above.

Statistical analysis

Numbers of experiments in the four groups (Control or DOX-treated WT and Nox2$^{-/-}$ mice) are based on data for coefficients of variation of relevant end-points in LV tissue analysis measured in prior studies (Zhao *et al*., 2010) and power calculations to allow detection of a 30% difference between groups with < 5% false negative error. *In vivo* analysis of cardiac structure and function was performed in all of the cohorts, to include most of the animals in the study. For gene expression profiling, three biological replicates were considered adequate to detect sufficient differences between the two samples (LV tissue from DOX-treated WT and Nox2$^{-/-}$ mice) to enable meaningful pathway analysis. HL-1 cardiomyocyte studies were performed using 6-8 preparations for each endpoint, but data for a whole experiment were discarded if on occasion, a response to DOX was not obtained. Where possible, data and statistical analysis comply with the recommendations on experimental design and analysis in pharmacology (Curtis *et al*., 2015).

Data were expressed as mean±SEM of *n* animals or tissue samples or cell preparations; values of n and number of technical replicates, if performed, are given in Figure and Table legends. Where replicates were conducted (Figures 8B and 9), these values were averaged to provide a single value contributing to the dataset. According to the design of the experiment, data were analysed using GraphPad Prism (Version 7.02) after application of the Brown-Forsythe test to examine homogeneity of variance using a parametric one- or two-factor ANOVA followed post-hoc, when indicated for a particular factor (when F achieved $P<0.05$), by a Bonferroni multiple comparison test for $n>2$ group comparisons, or if $n=2$, a paired or unpaired Student's *t* test. When data have been expressed as fold change for comparison purposes of readouts with different baselines, the Kruskal-Wallis test followed by Dunn's multiple comparison test was applied. In all cases, $P<0.05$ was considered to indicate statistical significance. Microarray data were analysed statistically as described in the relevant section.

RESULTS

Effects of DOX on cardiac function, LV remodelling and Nox2-dependent superoxide production

Echocardiography data taken from short axis M-mode recordings (Table 1) indicated that heart rate, LV wall thickness (IVSD, IVSS, LVPWD, LVPWS) and chamber dimensions (LVEDD,

LVESD) were unaltered comparing WT and Nox2$^{-/-}$ mice with or without DOX treatment. However, LV systolic function, as measured by fractional shortening, was decreased by DOX in WT but not in Nox2$^{-/-}$ mice. Similarly, diastolic dysfunction, quantified by a reduced MV E/A ratio versus that in controls, was evident in DOX-treated WT but not in Nox2$^{-/-}$ mice.

Examination of heart weight normalised to tibial length, which did not alter across groups, showed that DOX decreased LV mass in WT mice (Table 1), consistent with a cachectic effect, which was unaltered in Nox2$^{-/-}$ DOX-treated animals, compared to untreated control values. Histological analysis of cardiomyocyte cross-sectional area confirmed that the observed action of DOX on LV mass was due to a specific effect on the cardiomyocyte; compared to control values, this was reduced in WT, but not in Nox2$^{-/-}$ DOX-treated animals, indicating that DOX-induced cardiomyocyte atrophy is dependent upon Nox2 NADPH oxidase. Similarly, cardiomyocyte apoptosis was clearly exacerbated by DOX in LV sections from WT mice, in which the percentage of TUNEL-positive cells increased approximately 10-fold versus control, but this increase was considerably less (2-fold) in Nox2$^{-/-}$ mice (Figure 1A). Furthermore, the effect of DOX to increase activity of caspase 3/7 (key effector enzymes in the apoptotic process) in LV tissue from WT mice was largely attenuated in Nox2$^{-/-}$ mice (Figure 1B), confirming that DOX-induced cardiomyocyte apoptosis also appears to be Nox2-dependent.

As expected, a DOX-induced increase in LV NADPH-dependent superoxide production was observed in WT but not in Nox2$^{-/-}$ mice (Figure 1C), supporting the idea that Nox2-dependent superoxide generation plays an important role in DOX cardiotoxicity. Notably, superoxide generation was inhibited by the superoxide scavenger, Tiron, and the flavoprotein inhibitor, DPI, but not by the NOS inhibitor, L-NAME, the mitochondrial inhibitor, rotenone, or the xanthine oxidase inhibitor, oxypurinol (Figure 1D), suggesting that the observed signal particularly reflects NADPH oxidase-derived superoxide. This finding is consistent with increased expression of Nox2 mRNA (Figure 1E) and protein (Figure 1F) in LV tissue from WT DOX-treated animals versus controls. No differences in LV mRNA expression of NOS isoenzymes (NOS1, NOS2, NOS3), superoxide dismutases (SOD1, SOD2), glutaredoxin 1 and 2, catalase and glutathione peroxidase 1 were observed between DOX-treated WT and Nox2$^{-/-}$ mice (Figure S2).

Microarray profiling of LV tissue and selection of candidate gene

Samples of LV tissue from DOX-treated WT and Nox2$^{-/-}$ mice analysed using an Illumina MouseWG-6 v2.0 microarray showed acceptable read-outs in quality control assessment (Figure S3). Specifically, low, medium and high levels of hybridisation corresponded to signal

intensities, low and high stringency controls performed appropriately, successful secondary biotin staining was demonstrated and the signal for the negative (background) control was low. Furthermore, as expected, the signal level of housekeeping genes was high in comparison to the signal for 'all genes'. Using unsupervised hierarchical clustering, the six samples divided into two distinct groups based on mouse genotype (Figure 2A), with the heatmap representing differentially-expressed genes (Figure 2B). A similar separation was observed by principal component analysis (Figure 2C), whilst the genotype label accounted for 3.45 times more variation above any background noise (error) even before filtering, providing confidence in the arrays (Figure 2D). The number of genes selected for normalisation using the described filtering criteria was 16825 from the original number of 45281(43%) and normalised data from both WT and $Nox2^{-/-}$ samples demonstrated good correlation ($r \geq 0.99$) between biological replicates (Figure S4).

Based on an adjusted P value of <0.1 as the selection criterion, 152 mapped genes were found to be differentially expressed in LV tissue from WT versus $Nox2^{-/-}$ DOX-treated mice, and these are detailed in Table S2: (A) 92 upregulated genes and (B) 60 downregulated genes. Ingenuity Pathway Analysis highlighted a number of networks, which related to functional sub-sets. Figure 3 outlines the top 12 networks ranked on the basis of the number of focus molecules from the data set cross referenced against the library of networks. In the context of this investigation, the network ranked third highest is of particular interest - Cellular Assembly and Organisation, Cellular Function and Maintenance, and Cell Death and Survival, which included 18 differentially-regulated genes involved in these highly complex systems. Shown schematically in Figure 4A with highlighting of 15 genes particularly involved in Cell Death and Survival, it is not surprising to observe convergence on ERK1/ERK2, members of the MAPK super family which control cell fate through proliferation, apoptosis and necrosis pathways. Focusing on particular pathways involved in cardiomyocyte cell death that comprise Nox2 and activation by DOX, Figure 4B shows networks which include 6 relevant molecules: midkine and matrix metalloproteinase (MMP)-2 (MMP-2) in extracellular space; HSP1, heat shock factor binding protein 1, Mfn2; 3-phosphoinositide dependent protein kinase 1 (PDK1) in cytoplasm and peroxisome activated receptor gamma coactivator-1α (PGC-1α) in the nucleus. It should be noted that some of these genes were not necessarily differentially expressed based on high stringency single gene analysis (P<0.05), specifically MMP-2 and PDK1, but rather represented central nodes within the highlighted cell death signalling pathways (selected by our lower stringency approach, P<0.1; see Methods) which may be of

potential significance with regard to the observed effects of DOX. In an Ingenuity Downstream Effects Analysis, just two of the above mentioned genes were predicted to increase the function: upregulated Mfn2, a mitochondrial membrane protein, and downregulated midkine, a heparin-binding growth factor/cytokine. It is of note, however, that while upregulated PGC-1α was predicted to decrease the cell death function, it is a known activator of cardiac Mfn2 (Li *et al*., 2009). Indeed, as shown in Figure 4B, both PGC-1α and Mfn2 are implicated in DOX-related mechanisms, downstream of Nox2. In validation of the microarray data for Mfn2 and PGC-1α, showing fold changes in DOX-treated WT versus Nox2$^{-/-}$ mice of 1.5 and 1.7, respectively, mRNA analysis of LV tissue samples from all four experimental groups showed increased Mfn2 mRNA expression in DOX-treated WT versus control which was largely reduced in DOX-treated Nox2$^{-/-}$ mice with no difference in controls (Figure 5A); although not statistically significant, a similar trend was observed for PCG-1α mRNA expression (Figure 5B). Based on a robust microarray experiment and analysis, along with reproducibility of DOX-induced Mfn2 activation in a separate experimental set, and the supporting literature from the Ingenuity Knowledge Base, the potential of upregulated Mfn2 to influence cardiomyocyte survival was clearly apparent.

Investigation of Mfn2 involvement in Nox2-dependent signalling mechanisms underlying DOX-induced cardiomyocyte apoptosis

In order to assess the relevance of HL-1 cardiomyocytes as a model for study of mechanisms underlying DOX-induced oxidative stress, the temporal and concentration-dependent effects of DOX on protein expression/activity of Nox2 and Mfn2 were investigated. DOX at 5μM increased Nox2 protein at 24h (Figure 6A) and this was reflected in increased superoxide production at this concentration (Figure 6Bii), but not at a lower DOX concentration of 0.5μM (Figure 6Bi). Similarly, Mfn2 protein expression was increased by 5μM DOX at 24h (Figure 6C), which was subsequently confirmed in a time course experiment in which values were increased 2.1- and 2.3-fold at 24h and 48h, respectively. It was subsequently confirmed that treatment with a DOX concentration of 5μM for 24h produced a large increase in caspase 3/7 activity in HL-1 cardiomyocytes along with increased cell death, consistent with a pattern of apoptosis with secondary necrosis under these experimental conditions (Figure S5). A further reduction in cell viability at a higher DOX concentration (50μM) was not matched by an increased cytotoxicity readout. Furthermore, caspase 3/7 activity was reduced, indicating that when subjected to extreme stress, it is possible to miss the apoptotic window in which cells display their characteristic features. For this reason, lower DOX concentrations were used in

subsequent investigations of Nox2 and Mfn2 signalling in cell death mechanisms using gene silencing and pharmacological approaches. Initially, it was established that DOX-stimulated Nox2 protein expression could be abrogated using specific gene silencing, whilst knockdown of Mfn2 did not affect Nox2 protein level by comparison with the non-targeting negative control siRNA (Figure 7A). In contrast, DOX-stimulated Mfn2 protein expression was abolished using Mfn2 siRNA, whilst knockdown of Nox2 reduced Mfn2 protein level by ~50% (Figure 7B), indicating possible regulation of Mfn2 by Nox2.

Using the ApoTox-Glo™ Triplex assay, in an 'add-mix measure' format, the simultaneous measurement of cell viability and cytotoxicity produced unusual reductions of both of these measures when Ambion Silencer Select® negative control siRNA was used prior to DOX treatment: by comparison, targeting of Nox2 or Mfn2 was observed to produce increases in cytotoxicity, although not versus the DOX+LF2000 transfection control (Figure 8A). Cell viability as well as cell phenotype of a sample treated with negative control siRNA should remain comparable to that of an untreated sample, i.e. the transfection control. Furthermore, live and dead cell measures are normally inversely related, but here there was a concomitant decrease, not increase, in the cytotoxic response for negative control siRNA versus transfection control. The fact that there was a reduction in both readouts indicates the possibility that colour quenching of the fluorimetric readout (Niles *et al*. 2007) might have occurred under conditions of negative control siRNA transfection. Alternatively, an added cytotoxic effect by targeting a survival gene could produce a similar profile, as seen in Figure S5A-B. However, the negative control siRNA appeared to perform well in the caspase 3/7 assay, assessing activity by cleavage of the tetrapeptide sequence DEVD, such that there was no difference by comparison with the transfection control (Figure 8B). Gene-specific targeting of Nox2 or Mfn2 had no effect on the level of apoptosis induced by DOX under these conditions; it was therefore concluded that the level of knockdown may be insufficient and so an alternative experimental gene silencing strategy was adopted and a lower, likely less toxic concentration of DOX used. Indeed, in reverse-transfected HL-1 cardiomyocytes carried out in suspension using Dharmacon reagents, prior to seeding and DOX treatment (3μM), Mfn2 knockdown exceeded 90%. Subsequently, using the same caspase 3/7 assay, Mfn2 gene silencing significantly reduced activity versus a non-targeting siRNA (Figure 8D), although also reducing cell viability, assessed using the MTT colorimetric assay of cell metabolic activity (Figure 8C). Using a further index of caspase 3/7 activity, measurement by ELISA of the 85-kDa fragment from cleavage of PARP-1 at the DEVD site, knockdown of Mfn2 significantly reduced PARP-1 cleavage (Figure 8F), also

having a detrimental effect on cell integrity, measured using the Janus Green whole cell stain (Figure 8E).

Finally, the effect of pharmacological pan-NADPH oxidase inhibition on DOX-induced cardiotoxicity was studied in HL-1 cardiomyocytes using the triazolo pyrimidine, VAS2870, in the ApoTox-Glo™ assay. When used alone at the highest concentration (100μM), VAS2870 produced a significant reduction in cell viability, despite showing no cytotoxic effects or increases in apoptosis, as determined by caspase 3/7 activity. However, when used at a concentration of 50μM, which had no basal effects on the cells, VAS2870 markedly attenuated DOX-induced increases in both cytotoxicity and apoptosis, suggesting that these processes occur at least partly due to activation of NADPH oxidases.

DISCUSSION

Despite strong evidence supporting a role for Nox2-derived ROS in DOX-induced cardiotoxicity and their known involvement in established remodelling pathways, the precise mechanisms underlying Nox2 activation in this setting remain unknown. We sought, therefore, to identify and examine potential new mechanisms underlying NADPH oxidase-dependent downstream signalling in response to DOX treatment in cardiomyocytes.

As a basis for mechanistic studies, the initial objective was to characterise a murine model of DOX-induced cardiotoxicity in which Nox2-specific effects could be examined, and this was achieved using WT and $Nox2^{-/-}$ mice as in our previous study (Zhao *et al*., 2010), except that sampling was performed at 4 weeks rather than 8 weeks after initial treatment. Consistent with previous findings, genetic deletion of Nox2 protected mice against DOX-induced: (i) development of cardiac contractile dysfunction, specifically normalising systolic and diastolic function; (ii) cardiomyocyte atrophy, attenuating reductions in both LV mass and cardiomyocyte cross-sectional area; (iii) cardiomyocyte apoptosis, diminishing an increase of TUNEL-positive cells and of caspase 3/7 activity; and (iv) superoxide generation, reducing increased levels observed in WT mice. It was also established that DOX-induced ROS production in this setting was Nox2-derived, not due to modulation of endogenous antioxidant capacity or nitrosative stress, but consistent with DOX-stimulated expression of Nox2. Taken together, these current data consolidate convincing previous evidence that DOX-induced Nox2 NADPH oxidase-derived ROS are involved in progression towards cardiomyocyte apoptosis. As such, the experimental model of DOX-induced cardiotoxicity characterised here, examined

4 weeks post-treatment, appears suitable for investigation of novel genes and signalling pathways regulated by Nox2.

In subsequent microarray analysis comparing hearts from DOX-treated WT and Nox2$^{-/-}$ mice, Cell Death and Survival functions were found to contribute the most relevant and significant network to this dataset, in accordance with many previous findings relating to transcriptional analysis of cardiac DOX effects, identifying the importance of the protein ubiquitination response amongst others (Deng *et al*., 2007; Tokarska-Schlattner *et al*., 2010; Thandavarayan *et al*., 2010; Zhang *et al*., 2012; Sishi *et al*., 2013). In this study, we chose to specifically focus on the role of Nox2 as a novel aspect of DOX-mediated signalling in this setting. Probing the identified network for Nox2 and its interrelationships with pathways linked to cardiac cell fate highlighted a number of relevant genes, some of which would be expected to promote survival or contribute to cell death processes. For example, midkine exerts an acute cytoprotective effect in ischaemia-reperfusion injury, at least in part due to its anti-apoptotic effect (Kadomatsu *et al*., 2014); however, in DOX-treated WT hearts the expression of midkine was downregulated by comparison with Nox2$^{-/-}$ hearts, so the involvement of this growth factor in DOX-Nox2 apoptotic signalling may be questionable, although in a chronic treatment regime, it is possible that midkine may underlie an opposite adaptive mechanism. Similarly, downregulation of MMP-2 may be a late phase adaptation, since dysregulation of myocardial MMPs is generally regarded as an early contributory mechanism towards initiation and progression of heart failure. In particular, enhancement of MMP-2 in cardiomyocytes in response to DOX has been identified as redox-dependent (Spallarosa *et al*., 2006; Mukhopadhyay *et al*., 2009; Bartekova *et al*., 2015). Other significant changes induced by DOX and mediated by Nox2 indicated upregulation of gene expression and included increased phosphoinositide-dependent protein kinase-1, which is an important mediator of PI3K signalling, promoting cardiomyocyte survival via the PI3K-Akt pathway (An *et al*., 2013, Kitamura *et al*., 2014). Similarly, DOX-induced upregulation of HSP binding protein 1, which is implicated in maintaining redox homeostasis by upholding glutathione levels (Christians *et al*., 2012), may signify an attempt to promote survival by counteracting increased ROS production. Consistent with this argument, the upregulation of heat shock factor binding protein 1 by DOX, by repressing the transcriptional activity of heat shock factor-1 which can potentiate apoptosis through increased HSP25 (Vedam *et al*., 2010), might be expected to represent a counter-regulatory mechanism for cell survival.

The most exceptional finding from our gene array analysis was the identification of DOX-Nox2-mediated upregulation of Mfn2, a protein found in the outer mitochondrial membrane

which plays key roles in determining mitochondrial morphology and regulation of the fusion process. Changes in mitochondrial morphology have been linked to apoptotic cell death (Ong and Hausenloy, 2010) and Mfn2, independent of its pro-fusion properties, can bind with a pro-apoptotic member of the Bcl-2 family, Bax (Wang *et al*., 2010). Mfn2 is able to form a functional unit with the mitochondrial fission protein, dynamin-related protein 1, and Bax at the outer mitochondrial membrane to mediate apoptotic cell death (Karbowski *et al*., 2002). In agreement, a considerable number of studies identified in the Ingenuity Knowledge Base were found to support the idea that increased Mfn2 in cardiomyocytes predicted an adverse outcome, promoting cell death through apoptotic mechanisms. For example, Shen *et al*. (2007) demonstrated that Mfn2 mediates oxidative stress-induced apoptotic cell death in neonatal cardiomyocytes. Additionally, siRNA inhibition of Mfn2 prevented oxidative stress-induced apoptotic cell death in H9c2 cardiomyocytes (Karbowski *et al*., 2002). Strikingly, Mfn2 is reported to protect the heart against ischemia-reperfusion injury and ROS-mediated damage (Papanicolaou *et al*., 2011). It was therefore concluded that Mfn2 not only serves to maintain mitochondrial morphology in cardiomyocytes but also promotes mitochondrial permeability transition activation in response to Ca^{2+} stimulation or ROS generation, predisposing the cells to a number of cell-death-inducing stimuli. In substantiating our choice of Mfn2 as a primary candidate underlying DOX-stimulated Nox2 signalling, it was noted that PGC-1α, which was also identified from the array analysis as a potential gene involved in Nox2-dependent cardiomyocyte apoptosis, is reported to upregulate Mfn2 expression in response to metabolic demand (Soriano *et al*., 2006; Romanello and Sandri, 2013).

Further to identification of cardiomyocyte apoptosis as a major element in the DOX-induced cardiotoxic response and discovery that upregulation of Mfn2 was strongly linked, the final part of this investigation examined the functional relevance of Mfn2 and its relationship to Nox2 in cell death processes using gene silencing in HL-1 cardiomyocytes. Important characteristics of the mouse model used in mRNA profiling of cardiac DOX-Nox2 signalling were replicated in HL-1 cardiomyocytes treated with DOX (5μM), namely increased superoxide production, and upregulation of Nox2 and Mfn2 protein expression. Furthermore, the cell death profile induced by DOX in this setting is consistent with increased apoptosis leading to secondary necrosis, whilst the concentrations of DOX used in this study (0.5-5μM) are relevant to plasma levels found clinically up to 1h post-treatment (0.1-10μM) (Anderson et al., 1999). In a pharmacological approach, the observed effects of the pan-NADPH oxidase inhibitor, VAS2870, on DOX (5μM)-induced cell death add weight to the involvement of Nox2 signalling

in this model, although it should be noted that VAS2870 can exert Nox2-independent actions (Gatto *et al*., 2013) and is cytotoxic at high concentrations (Zielonka *et al*., 2014), which we observed at 100µM. However, at a concentration of 50µM, which maintained cell viability, VAS2870 was shown to reduce both cytotoxicity and caspase 3/7 activity.

Again using a DOX concentration of 5µM and applying specific gene silencing, ~50% knockdown of the Nox2 and Mfn2 proteins was achieved in HL-1 cardiomyocytes and this was increased to >90% by adopting a reverse transfection protocol. Similar studies have reported the effective use of siRNAs to knockdown both Nox and Mfn2 and inhibit ROS production and apoptosis in cardiac cells, including HL-1 cardiomyocytes (Yeh *et al*., 2011), H9c2 cardiomyocytes, (Shen *et al*., 2007), cultured neonatal rat cardiomyocytes (Papanicolaou *et al*., 2011) and mouse ventricular cells (Moe *et al*., 2011). However, while this investigation found no changes in apoptosis in DOX-treated HL-1 cardiomyocytes in the presence of Nox2 or Mfn2 knockdown, it is possible that efficacy of transfection may have influenced the measured endpoint. Indeed, highly oxidative tissues such as the heart require constant energy production, and as mitochondria are the powerhouse of the cardiomyocyte comprising a large proportion of cytoplasmic volume, it is possible that there is such a high level of Mfn2 expression in HL-1 cardiomyocytes that the observed effects of Mfn2 siRNA on cell apoptosis may have underestimated the involvement of Mfn2 (Bach *et al*., 2003; Papanicolaou *et al*., 2011). Indeed, when a higher level of knockdown was achieved, a lack of Mfn2 corresponded with reduction of caspase 3/7 activity, assessed by both DEVD and PARP-1 cleavage. This must be countered, however, by recognition that there was no evidence of reduced cytotoxicity, assessed by the dead cell protease assay (R110). In fact, there was tendency towards reduced cell viability in all three measures, which included two of membrane integrity (live cell protease assay - AFC, Janus Green Whole Cell) and also mitochondrial activity (MTT). It appears, therefore, that in an environment associated with extreme loss of Mfn2 activity, HL-1 cardiomyocytes are more likely to undergo necrotic transformation; it is also possible that impairment of autophagic processes will impact on mitochondrial quality control (Andres *et al*., 2015). As further information emerges, it seems that there is equivalent evidence that maintained levels of Mfn2 may be required to counteract cell oxidative stress; for example, further to ROS induced by hypoxia/reoxygenation in cardiomyocytes, up-regulated Mfn2 expression prevented imbalance in mitochondrial dynamics (Dong *et al*., 2016). Loss of Mfn2 also delayed membrane depolarisation in isolated cardiomyocytes from adult $Mfn2^{-/-}$ mice, leading to the suggestion that Mfn2 may function to control mitochondrial permeability transition pore opening

(Papanicolaou *et al*., 2011). Similarly, cardiac-specific deletion of Mfn2 produced dissipation of mitochondrial membrane potential and elevated ROS production (Chen *et al*., 2012), whilst overexpression of Mfn2 was found to increase the percentage of cells containing elongated mitochondria, thereby reducing mitochondrial permeability transition pore opening and cell death after simulated ischemia/reperfusion injury (Ong *et al*., 2010). It also appears that Mfn2 serves an essential role in maintaining mitochondrial coenzyme Q levels in mouse hearts, thereby promoting optimal function of the respiratory chain (Mourier *et al*., 2015).

In summary, therefore, it is probably true to say that the participation of Mfn2 in control of cardiomyocyte life or death is complex and depends upon its level of expression (Schrepfer and Scorrano, 2016). Nonetheless, the results of this study clearly demonstrate that while DOX through NADPH oxidase signalling in general can have a detrimental effect on cardiomyocyte survival, a particular Nox2-stimulated pathway including Mfn2 may signify an attempt to maintain mitochondrial biogenesis.

In consideration of this novel premise, it must be taken into account that our investigation has limitations, primarily that the mouse model may not truly reflect salient features of DOX-induced cardiotoxicity in humans, because of differences in drug metabolism and/or cardiac structure and function, and sensitivity to cardiac injury, all of which may be influenced by aging and co-morbidities (Madonna *et al*., 2015). Preferentially, studies in human cardiac tissue would be performed, but being largely unobtainable, there has been increasing interest in disease modelling using human embryonic stem cell and induced pluripotent stem cell-derived cardiomyocytes (Madonna *et al*., 2016, Maillet *et al*., 2016), although this also is not without criticism. Another approach is to examine peripheral blood mononuclear cells (PBMCs), in which the transcriptome in DOX-exposed PBMCs is highly similar to that in treated cardiomyocytes (Todorova *et al*., 2012). Of particular relevance to the findings of the current study, it would be of interest to extend investigation of the role of Mfn2 after DOX treatment using patient-derived PBMCs, since systemic mitochondrial pathologies have been shown to correlate in PBMCs and in cardiac tissues (Lipshultz *et al*., 2016).

The potential for activation of Mfn-2 as a therapeutic strategy for cardioprotection in ischaemic disease and heart failure has recently received considerable attention (Ong *et al*., 2014; Walters *et al*., 2016). This has been intensified by recognition that Mfn2 may play a critical role in cell-based therapies promoting the differentiation of stem cells into cardiomyocytes (Kasahara *et al*., 2013; Suliman *et al*., 2016). Indeed, DOX-induced cardiomyopathy is associated with depletion and senescence of the cardiac progenitor cell pool in both rat and human hearts,

permanently impairing their function (de Angelis *et al*., 2010; Piegari *et al*., 2013). Therefore, a pharmacological strategy involving Mfn2 that could potentially prevent degeneration of both adult cardiac cells and the resident stem cell pool seems an attractive idea. Such an approach may be enabled by the identification of a small natural molecule, 15-oxospiramilactone which, through inhibition of a mitochondria-localized deubiquitinase, increases Mfn2 activity (Yue *et al*., 2014), although effects have yet to be demonstrated in relevant models that could indicate potential targeting of this mechanism for translation to the clinic.

AUTHOR CONTRIBUTIONS

D.McL, Y.Z, K.M.O'N, D.J.G, B.J.McD conceived and designed the experiments; D.McL, K.M.O'N, Y.Z., K.S.E, A.M.K performed the experiments; D.McL, Y.Z, K.M.O'N, K.S.E, P.D.D, D.J.G, B.J.McD analysed the data and drafted relevant text; D.McL, D.J.G and B.J.McD wrote the manuscript.

CHANGE OF AUTHOR AFFILIATION

Dr Youyou Zhao is now at Nestlé Research Centre Beijing, Building 5, No. 5 Dijin Road, Haidian District, Beijing, 100095, China.

ACKNOWLEDGEMENTS

This work was supported by the British Heart Foundation (Project Grant PG/06/112 to D.J.G and B.J.McD) and a PhD Studentship from the Department for Employment and Learning (NI).

CONFLICTS OF INTEREST

None.

REFERENCES

Alexander SP, Fabbro D, Kelly E, Marrion N, Peters JA, Benson HE et al. (2015). The Concise Guide to PHARMACOLOGY 2015/16: Enzymes. *Br J Pharmacol* **172**: 6024-6109.

An T, Zhang Y, Huang Y, Zhang R, Yin S, Guo X et al. (2013) Neuregulin-1 protects against doxorubicin-induced apoptosis in cardiomyocytes through an Akt-dependent pathway. *Physiol Res* **62**: 379-385.

Anderson A, Holte H, Slordal L (1999) Pharmacokinetics and metabolism of doxorubicin after short-term infusions in lymphoma patients. *Cancer Chemother Pharmacol* **44**: 422-426.

Andres AM, Stotland A, Queliconi BB, Gottlieb, RA (2015) A time to reap, a time to sow: Mitophagy and biogenesis in cardiac pathophysiology. *J Mol Cell Cardiol* **78**: 62-72.

Bach D, Pich S, Soriano FX, Vega N, Baumgartner B, Oriola J et al. (2003) Mitofusin-2 determines mitochondrial network architecture and mitochondrial metabolism. A novel regulatory mechanism altered in obesity. *J Biol Chem* **278**: 17190-17197.

Bartekova M, Simoncikova P, Fogarassyova M, Ivanova M, Okruhlicova L, Tribulova N et al. (2015) Quercetin improves postischemic recovery of heart function in doxorubicin-treated rats and prevents doxorubicin-induced matrix metalloproteinase-2 activation and apoptosis induction. *Int J Mol Sci* **16**: 8168-8185.

Bloom MW, Hamo CE, Cardinale D, Ky B, Nohria A, Baer L et al. (2016) Cancer therapy-related cardiac dysfunction and heart failure Part 1: Definitions, pathophysiology, risk Factors, and imaging. *Circ Heart Fail* **9**: e002661.

Cardinale D, Colombo A, Bacchiani G, Tedeschi I, Meroni CA, Veglia F et al., (2015) Early detection of anthracycline cardiotoxicity and improvement with heart failure therapy. *Circulation* **131**: 1981-1988.

Carvalho FS, Burgeiro A, Garcia R, Moreno AJ, Carvalho RA, Oliveira PJ (2014) Doxorubicin-induced cardiotoxicity: from bioenergetic failure and cell death to cardiomyopathy. *Med Res Rev* **34**: 106-135.

Chen Y, Csordas G, Jowdy C, Schneider, TG, Csordas N, Wang W et al. (2012) Mitofusin 2-containing mitochondrial-reticular microdomains direct rapid cardiomyocyte bioenergetic responses via interorganelle Ca^{2+} crosstalk. *Circ Res* **111**: 863-875.

Christians ES, Ishiwata T, Benjamin, IJ (2012) Small heat shock proteins in redox metabolism: Implications for cardiovascular diseases. *Int J Biochem Cell Biol* **10**: 1632-1645.

Curtis MJ, Bond RA, Spina D, Ahluwalia, A, Alexander, SPA, Giembycz MA et al. (2015) Experimental design and analysis and their reporting: new guidance for publication in BJP. *Br J Pharmacol* **172**: 3461-3471.

De Angelis A, Piegari E, Cappetta D, Marino L, Filippelli A, Berrino L et al. (2010) Anthracycline cardiomyopathy is mediated by depletion of the cardiac stem cell pool and is rescued by restoration of progenitor cell function. *Circulation* **121**: 276-292.

Deidda M, Madonna R, Mango R, Pagliaro P, Bassereo PP, Cugusi L et al. (2016) Novel insights in pathophysiology of antiblastic drugs-induced cardiotoxicity and cardioprotection. *J Cardiovasc Med* **17** (Suppl 1): e76-e83.
Deng S, Kulle B, Hosseini M, Schlüter G, Hasenfuss G, Wojnowski L et al. (2007) Dystrophin-deficiency increases the susceptibility to doxorubicin-induced cardiotoxicity. *Eur J Heart Fail* **9**: 986-994.

Dong GT, Chen TB, Ren XC, Zhang, ZF, Huang, WX, Liu L et al. (2016) Rg1 prevents myocardial hypoxia/reoxygenation injury by regulating mitochondrial dynamics imbalance via modulation of glutamate dehydrogenase and mitofusin 2. *Mitochondrion* **26**: 7-18.

Du P, Kibbe WA, Lin SM (2008) Lumi: a pipeline for processing Illumina microarray. *Bioinformatics* **24**: 1547-1548.

Gatto GJ, Ao ZH, Kearse MG, Zhou M, Morales CR, Daniels, E et al. (2013) NADPH oxidase-dependent and -independent mechanisms of reported inhibitors of reactive oxygen generation. *J Enz Inhib Med Chem* **28**: 95-102.

Ghigo A, Mingchuan L, Hirsch E (2016) New signal transduction paradigms in anthracycline-induced cardiotoxicity. *Biochim Biophys Acta* **1863**: 1916-1925.

Gilleron M, Marechal X, Montaigne D, Franczak J, Neviere R, Lancel, S (2009) NADPH oxidases participate to doxorubicin-induced cardiac myocyte apoptosis. *Biochem Biophys Res Comm* **388**: 727-731.

Grieve DJ, Byrne JA, Siva A, Layland J, Johar S, Cave AC et al. (2006) Involvement of the nicotinamide adenosine dinucleotide phosphate oxidase isoform Nox2 in cardiac contractile dysfunction occurring in response to pressure overload. *J.Am Coll Cardiol* **47**: 817-826.

Ito H, Miller SC, Billingham ME, Akimoto H, Torti SV, Wade, R et al. (1990) Doxorubicin selectively inhibits muscle gene-expression in cardiac-muscle-cells in vivo and in vitro. *Proc Nat Acad Sci USA* **87**: 4275-4279.

Kadomatsu K, Bencsik P, Gorbe A, Csonka C, Sakamoto K, Kishida S et al. (2014) Therapeutic potential of midkine in cardiovascular disease. *Br J Pharmacol* **171**: 936-944.

Karbowski M, Lee YJ, Gaume B, Jeong SY, Frank S, Nechushtan A et al. (2002) Spatial and temporal association of Bax with mitochondrial fission sites, Drp1, and Mfn2 during apoptosis. *J Cell Biol* **159**: 931-938.

Kasahara A, Cipolat S, Chen Y, Dorn GW 2nd, Scorrano L (2013) Mitochondrial fusion directs cardiomyocyte differentiation via calcineurin and notch signaling. *Science* **342**: 734–737.

Kitamura Y, Koide M, Akakabe Y, Matsuo K, Shimoda Y, Soma Y et al. (2014) Manipulation of cardiac phosphatidylinositol 3-kinase (PI3K)/Akt Signaling by apoptosis regulator through modulating IAP Expression (ARIA) regulates cardiomyocyte death during doxorubicin-induced cardiomyopathy. *J Biol Chem* **289**: 2788-2800.

Kobayashi S, Volden P, Timm D, Mao K, Xu X, Liang Q (2010) Transcription factor GATA4 inhibits doxorubicin-induced autophagy and cardiomyocyte death. *J Biol Chem* **285**:793-804.

Kuhn K, Baker SC, Chudin E, Lieu MH, Oeser S, Bennett H et al. (2004) A novel, high-performance random array platform for quantitative gene expression profiling. *Genome Res* **14**: 2347-2356.

Li Y, Yin R, Liu J, Wang P, Wu S, Luo J et al. (2009) Peroxisome proliferator-activated receptor delta regulates mitofusin 2 expression in the heart. *J Mol Cell Cardiol* **46**: 876-882.

Lin SM, Du P, Huber W, Kibbe WA (2008) Model-based variance-stabilizing transformation for Illumina microarray data. *Nucleic Acids Res* **36**: e11.

Lipshultz SE, Anderson LM, Miller T, Gerschenson M, Stevenson KE. Neuberg DS et al. (2016) Impaired mitochondrial function is abrogated by dexrazoxane in doxorubicin-treated childhood acute lymphoblastic leukemia survivors. *Cancer* **122**: 946-953.

Liu L, Zhang X, Qian B, Min X, Gao X, Li C (2007) Over-expression of heat shock protein 27 attenuates doxorubicin-induced cardiac dysfunction in mice. *Eur J Heart Fail* 9: 762-769.

Madamanchi NR, Runge MS (2013) Redox signaling in cardiovascular health and disease. *Free Radic Biol Med* **61**: 473-501.

Madonna R, Cadeddu C, Deidda M, Mele D, Monte I, Novo G et al. (2015) Improving the preclinical models for the study of chemotherapy-induced cardiotoxicity: a Position Paper of the Italian Working Group on Drug Cardiotoxicity and Cardioprotection. *Heart Fail Rev* **20**: 621-631.

Madonna R, Cadeddu C, Deidda M, Spallarossa P, Zito C, Mercuro G (2016) Modelling chemotherapy-induced cardiotoxicity by human pluripotent stem cells. *Curr Drug Targets* **17**: 1-5.

Maillet A, Tan K, Chai X, Sadananda SN, Mahta A, Ooi J et al. (2016) Modeling doxorubicin-induced cardiotoxicity in human pluripotent stem cells derived cardiomyocytes. *Sci Rep* **6**: 25333.

McGrath JC, Lilley E (2015) Implementing guidelines on reporting research using animals (ARRIVE etc.): new requirements for publication in BJP. *Br J Pharmacol* **172**: 3189-3193.

Moe KT, Yin NO, Naylynn TM, Khairunnisa K, Wutyi MA, Gu Y et al. (2011) Nox2 and Nox4 mediate tumour necrosis factor-α-induced ventricular remodelling in mice. *J Cell Mol Med* **15**: 2601-2613.

Mourier A, Motori E, Brandt T, Lagouge M, Atanassov I, Galinier A et al. (2015) Mitofusin 2 is required to maintain mitochondrial coenzyme Q levels. *J Cell Biol* **4**: 429-442.

Mukhopadhyay P, Rajesh M, Bátkai S, Kashiwaya Y, Haskó G, Liaudet L (2009) Role of superoxide, nitric oxide, and peroxynitrite in doxorubicin-induced cell death in vivo and in vitro. *Am J Physiol Heart Circ Physiol* **296**: 1466-1483.

Niles A, Moravec RA, Eric Hesselberth P, Scurria MA, Daily WJ, Riss TL (2007) A homogeneous assay to measure live and dead cells in the same sample by detecting different protease markers. *Anal Biochem* **366**: 197-206.

Ong SB, Hausenloy DJ (2010) Mitochondrial morphology and cardiovascular disease. *Cardiovasc Res* **88**: 16-29.

Ong SB, Kalhoran SB, Cabrera-Fuentes HA, Hausenloy DJ (2015) Mitochondrial fusion and fission proteins as novel therapeutic targets for treating cardiovascular disease. *Eur J Pharmacol* **763**: 104-114.

Ong SB, Subrayan S, Lim SY, Yellon DM, Davidson SM, Hausenloy DJ (2010) Inhibiting mitochondrial fission protects the heart against ischemia/reperfusion injury. *Circulation* **121**: 2012-2022.

Papanicolaou KN, Khairallah RJ, Ngoh GA, Chikando A, Luptak I, O'Shea KM et al. (2011) Mitofusin-2 maintains mitochondrial structure and contributes to stress-induced permeability transition in cardiac myocytes. *Mol Cell Biol* **31**: 1309-1328.

Pawson AJ, Sharman JL, Benson HE, Faccenda E, Alexander SP, Buneman OP et al. (2014). The IUPHAR/BPS guide to PHARMACOLOGY: an expert-driven knowledge base of drug targets and their ligands. *Nucleic Acids Res* **42**: D1098–D1106.

Piegari E, De Angelis A, Cappetta D, Russo R, Esposito E, Costantino S et al. (2013) Doxorubicin induces senescence and impairs function of human cardiac progenitor cells. *Basic Res Cardiol* **108**: 334-351.

Poizat C, Puri PL, Bai Y, Kedes L (2005) Phosphorylation-dependent degradation of p300 by doxorubicin-activated p38 mitogen-activated protein kinase in cardiac cells. *Mol Cell Biol* **25**: 2673-2687.

Pollock JD, Williams DA, Gifford MA, Li LL, Du X, Fisherman J et al. (1995) Mouse model of X-linked chronic granulomatous disease, an inherited defect in phagocyte superoxide production. *Nat Genet* **9**: 202-209.

Romanello V, Sandri M (2013) Mitochondrial biogenesis and fragmentation as regulators of protein degradation in striated muscles. *J Mol Cell Cardiol* **55**: 64-72.

Schrepfer E, Scorrano, L (2016) Mitofusins, from mitochondria to metabolism. *Mol Cell* **61**: 683-694.

Shen T, Zheng M, Cao C, Chen C, Tang J, Zhang W et al. (2007) Mitofusin-2 is a major determinant of oxidative stress-mediated heart muscle cell apoptosis. *J Biol Chem* **282**: 23354-23361.

Sishi BJ, Loos B, van Rooyen J, Engelbrecht, AM (2013) Doxorubicin induces protein ubiquitination and inhibits proteasome activity during cardiotoxicity. *Toxicology* **309**: 23-29.

Soriano FX, Liesa M, Bach D, Chan DC, Palacín M, Zorzano A (2006) Evidence for a mitochondrial regulatory pathway defined by peroxisome proliferator-activated receptor-gamma coactivator-1 alpha, estrogen-related receptor-alpha, and mitofusin 2. *Diabetes* **55**: 1783-1791.

Spallarossa P, Altieri P, Garibaldi S, Ghigliotti G, Barisione C, Manca V (2006) Matrix metalloproteinase-2 and -9 are induced differently by doxorubicin in H9c2 cells: The role of MAP kinases and NAD(P)H oxidase. *Cardiovasc. Res* **69**: 736-745.

Spallarossa P, Maurea N, Cadeddu C, Madonna R, Mele D, Monte I et al. (2016) A recommended practical approach to the management of anthracycline-based chemotherapy cardiotoxicity: an opinion paper of the working group on drug cardiotoxicity and cardioprotection, Italian Society of Cardiology. *J Cardiovasc Med* **17** (Suppl 1): e84-e92.

Sterba M, Popelova, O, Vavrova A, Jirkovsky E, Kovarikova, P, Gersl, V et al. (2013) Oxidative stress, redox signaling, and metal chelation in anthracycline cardiotoxicity and pharmacological cardioprotection. *Antioxid Redox Signal* **18**: 899-929.

Suliman HB, Zobi F, Piantadosi CA (2016) Heme oxygenase-1/carbon monoxide system and embryonic stem cell differentiation and maturation into cardiomyocytes. *Antioxid Redox Signal* **24**: 345-360.

Suzuki YJ (2011) Cell signalling pathways for the regulation of GATA-4 transcription factor: implications for cell growth and apoptosis. *Cell Signal* **23**: 1094-1099.

Thandavarayan RA, Watanabe K, Sar IF, Ma M, Lakshmanan AP, Giridharan VV et al. (2010) Modulation of doxorubicin-induced cardiac dysfunction in dominant-negative p38α mitogen-activated protein kinase mice. *Free Radic Biol Med* **49**: 1422-1431.

Todorova VK, Beggs ML, Delongchamp RR, Dhakal I, Makhoul I, Wei JY et al. (2012) Transcriptome profiling of peripheral blood cells identifies potential biomarkers for doxorubicin cardiotoxicity in a rat model. *PLoS One* **7**: e48398.

Tokarska-Schlattner M, Lucchinetti E, Zaugg M, Kay L, Gratia S, Guzun R et al (2010) Early effects of doxorubicin in perfused heart: transcriptional profiling reveals inhibition of cellular stress response genes. *Am J Physiol Regul Integr Comp Physiol* **298**: 1075-1088.

Tokarska-Schlattner M, Zaugg M, Zuppinger C, Walliman T, Schlattner U (2006) New insights into doxorubicin-induced cardiotoxicity: The critical role of cellular energetics. *J Mol Cell Cardiol* **41**: 389-405.

van Dalen EC, Caron HN, Dickinson HO, Kremer LC (2011) Cardioprotective interventions for cancer patients receiving anthracyclines. *Cochrane Database Syst Rev* **6**: CD003917.

Vedam K, Nishijima Y, Druhan LJ, Khan M, Moldovan NI, Zweier JL et al. (2010) Role of heat shock factor-1 activation in the doxorubicin-induced heart failure in mice. *Am J Physiol Heart Circ Physiol* **298**: H1832-1841.

Vincent DT, Ibrahim YF, Espey MG, Suzuki, YJ (2013) The role of antioxidants in the era of cardio-oncology. *Cancer Chemother Pharmacol* **72**: 1157-1168.

Walters JW, Amos D, Ray K, Santanam N (2016) Mitochondrial redox status as a target for cardiovascular disease. *Current Opinion Pharmacol* **27**: 50–55.

Wang L, Zhang TP, Zhang Y, Bi HL, Guan XM, Wang HX et al. (2016) Protection against doxorubicin-induced myocardial dysfunction in mice by cardiac-specific expression of carboxyl terminus of hsp70-interacting protein. *Sci Rep* **6**: 28399.

Wang W, Cheng X, Lu J, Wei J, Fu G, Zhu F et al. (2010) Mitofusin-2 is a novel direct target of p53. *Biochem Biophys Res Commun* **400**: 587-592.

Wojnowski L, Kulle B, Schirmer M, Schluter G, Schmidt A, Rosenberger A et al. (2005) NAD(P)H oxidase and multidrug resistance protein genetic polymorphisms are associated with doxorubicin-induced cardiotoxicity. *Circulation* **112**: 3754-3762.

Yeh YH, Kuo CT, Chan TH, Chang GJ, Qi XY, Tsai F et al. (2011) Transforming growth factor-β and oxidative stress mediate tachycardia-induced cellular remodelling in cultured atrial-derived myocytes. *Cardiovasc Res* **91**: 62-70.

Yoshida M, Shiojima I, Ikeda H, Komuro I (2009) Chronic doxorubicin cardiotoxicity is mediated by oxidative DNA damage-ATM-p53-apoptosis pathway and attenuated by pitavastatin through the inhibition of Rac1 activity. *J Mol Cell Cardiol* **47**: 698-705.

Yue W, Chen Z, Liu H, Yan C, Chen M, Feng D et al. (2014) A small natural molecule promotes mitochondrial fusion through inhibition of the deubiquitinase USP30. *Cell Res* **24**: 482-498.

Zhang S, Liu X, Bawa-Khalfe T, Lu LS, Lyu YL, Liu LF et al. (2012) Identification of the molecular basis of doxorubicin-induced cardiotoxicity. *Nat Med* **11**: 1639-1642.

Zhao Y, McLaughlin D, Robinson E, Harvey AP, Hookham MB, Shah AM et al. (2010) Nox2 NADPH oxidase promotes pathologic cardiac remodeling associated with doxorubicin chemotherapy. *Cancer Res* **70**: 9287-9297.

Zielonka J, Cheng G, Zielonka M, Ganesh T, Sun AM, Joseph J et al. (2014) high-throughput assays for superoxide and hydrogen peroxide: design of a screening workflow to identify inhibitors of NADPH oxidases. *J Biol Chem* **289**: 16176-16189.

FIGURE LEGENDS

Figure 1

Effects of DOX on cardiomyocyte apoptosis, LV superoxide production, and Nox2 mRNA and protein expression in WT and Nox2$^{-/-}$ (KO) mice. (A) TUNEL-positive cardiomyocyte nuclei in LV sections quantified by digital image analysis (n=6, 80 cells in each). (B) Caspase 3/7 activity in LV tissue, expressed as relative light units (RLU; n=5). (C) NADPH-dependent superoxide production analysed in LV membrane fractions by lucigenin-enhanced chemiluminescence (n=6). (D) Effects of selective ROS inhibitors on superoxide production in WT samples (n=6). (E) Nox2 mRNA expression assessed in LV tissue by real-time TaqMan RT-PCR (n=15-WT, n=9-KO). (F) Representative Western blot of Nox2 protein expression in LV homogenate (M, MCF-7 cell lysate positive control; WTC, WT control; WTD, WT DOX-treated; KOC, KO control; KOD, KO DOX-treated; HPRT, Hypoxanthine-guanine phosphoribosyltransferase endogenous control) and its quantification (n=6). Data (Control □, DOX ■) are shown as mean (±SEM) and analyses performed using a two-factor ANOVA followed by unpaired Student's *t* test (A, B, C) or Kruskal-Wallis test with Dunn's post-hoc test for Control or DOX (D) or unpaired Student's *t* test with Walsh's correction to account for unequal variances (E, F). *P<0.05 vs WT Control; $^{\#}$P<0.05 vs WT DOX.

Figure 2

Microarray profiling of LV sample replicates from WT and Nox2$^{-/-}$ (KO) DOX-treated mice. (A) Unsupervised hierarchical clustering, (B) Heatmap representation of differentially expressed genes generated, (C) Principal component analysis (PCA) and (D) Signal to noise ratio for tissue samples (ID) compared to background, generated using Partek Genomics Suite, using 3 mice in each group.

Figure 3

Network analysis of genes differentially regulated in LV tissue from WT vs. Nox2$^{-/-}$ DOX-treated mice. 152 genes (using cut-off of adjusted P<0.1) were analysed using Ingenuity Pathway Analysis software. Expression of genes in bold are significantly differentially regulated between groups (red arrows indicate upregulation and green arrows downregulation); genes not in bold are implicated in the networks but are not differentially regulated.

Figure 4

Identification of differentially regulated genes within the Cellular Assembly and Organisation, Cellular Function and Maintenance, and Cell Death and Survival network. (A) Gene interactions for Network ID 3 in Figure 3 were generated by Ingenuity Pathway Analysis software. Red coloured genes are significantly upregulated and green coloured genes downregulated; the more intense the colour, the higher the level of differential gene expression; uncoloured molecules are not differentially expressed but involved in the network. Solid lines indicate a direct interaction, dashed lines an indirect interaction. The overlay highlights genes specifically involved in Cell Death and Survival mechanisms: ACTB, β-actin; AGRN aagrin; AHSA1, activator of HSP90 ATPase activity 1; DAG1, dystroglycan 1; DKK3, dickkopf WNT signalling pathway inhibitor 3; HSPB1, heat shock protein binding protein 1 ; INPPL1, inositol polyphosphate phosphatase like 1; MDK, midkine transcript variant 3; MFN2, mitofusin 2; NDRG2, N-myc downstream regulated gene 2; PDPK1, 3-phosphoinositide dependent protein kinase 1; PLD1, phospholipase D1; PP2A, protein phosphatase 2; RABL6, RAB member RAS oncogene family-like 6; SYNM, synemin. (B) Cellular location of differentially-regulated genes which interact with DOX (extracellular) and Nox2 (CYBB; at the cytosolic-plasma membrane junction). Solid lines indicate a direct interaction, dashed lines an indirect interaction. Seven genes specifically involved in cardiomyocyte cell death are highlighted in blue: HSBP1, heat shock factor binding protein 1; HSPD1, heat shock protein D1; MDK, midkine transcript variant 3; MFN2, mitofusin 2; MMP2, matrix metallopeptidase 2; PDPK1, 3-phosphoinositide dependent protein kinase 1; PPARGC1A, peroxisome activated receptor gamma coactivator 1 alpha.

Figure 5

Candidate gene expression in LV tissue from WT and Nox2$^{-/-}$ (KO) DOX-treated mice. Real-time RT-PCR mRNA expression analysis of (A) Mfn2 (n=6) and (B) PGC-1α (n=9). Data (Control □, DOX ■) are shown as mean (±SEM) and analyses performed using a two-factor ANOVA followed by unpaired Student's t-test. $^{\#}P<0.05$ vs WT DOX.

Figure 6

Effect of DOX concentration and time of incubation on superoxide production, gene and protein expression in HL-1 cardiomyocytes. (A) Representative Western blot showing effects of DOX concentration on Nox2 protein expression at 24h and its quantification (n=5); (B) NADPH oxidase activity in the presence of (i) 0.5μM and (ii) 5μM DOX assessed by lucigenin-

enhanced chemiluminescence over 24h (both n=5); (C) Representative Western blot showing effects of DOX concentration on Mfn2 protein expression at 24h and its quantification (n=5). HPRT, Hypoxanthine-guanine phosphoribosyltransferase endogenous control); H, HeLa cell lysate positive control; M, MCF-7 cell lysate positive control; C, Control (normal medium). Data (Control □, DOX ■) are shown as mean (±SEM) and analyses performed using one-factor ANOVA (Kruskal-Wallis test) and Dunn's post-hoc test (A, C) or two-factor ANOVA with paired Student's t-test, as indicated (B). *P<0.05 vs Control.

Figure 7

Effect of siRNA gene silencing on DOX-induced Nox2 and Mfn2 protein expression in HL-1 cardiomyocytes. Representative Western blots of protein expression induced by DOX (5μM) at 24h under control conditions and in the presence of Silencer Select® siRNAs (Mfn2, Nox2, Universal negative control, 200M) and its quantification: (A) Nox2 (n=5) and (B) Mfn2 (n=6). H, HeLa cell lysate positive control; M, MCF-7 cell lysate positive control; C, Control (normal medium); D, DOX; Mfn2, Mfn2 siRNA; Nox2, Nox2 siRNA; Neg., negative control siRNA. Data are shown as mean values (±SEM) and analyses performed using one-factor ANOVA (Kruskal-Wallis test) and Dunn's post-hoc test. *P<0.05 vs Control; $^{\#}$P<0.05 vs negative control DOX + siRNA.

Figure 8

Effect of Mfn2 and Nox2 gene silencing on HL-1 cardiomyocyte survival. ApoTox-Glo™ Triplex assay of cells incubated with normal medium (Control, C) or with DOX (5μM) for 24h without or with previous transfection using LF2000 alone or with Silencer Select® Universal Negative Control, Mfn2 or Nox2 siRNAs (200M) for 24h detected by fluorescence: (A) Cell viability (AFC) and cytotoxicity (R110); and by luminescence: (B) Caspase 3/7 activity (cleavage of DEVD; all n=5, 3-4 replicates in each experiment which were averaged to provide a single value): using reverse transfection with Dharmafect (DFCT) and ON-TARGET plus SMARTpool siRNAs (24h, 100nM) and DOX (3μM, 24h): (C) Colorimetric readout of cell viability (MTT), (D) Caspase-Glo 3/7 assay of caspase 3/7 activity (DEVD); (E) Colorimetric readout of cell viability (Janus Green whole cell stain); (F) Colorimetric In-Cell ELISA of cleaved PARP-1 (all n=7). RLU, relative light units. Data are shown as mean value (±SEM) and analyses performed using a one-factor ANOVA followed by Bonferroni post-hoc test. *P<0.05 vs. Control or Control + transfection agent; $^{+}$P<0.05 DOX + -ve siRNA vs DOX + transfection agent; $^{\#}$P<0.05 DOX + Nox2 or Mfn2 siRNA vs DOX + –ve siRNA.

Figure 9

Effect of pharmacological NADPH oxidase inhibition on HL-1 cardiomyocyte survival. ApoTox-Glo™ Triplex assay of cells incubated with normal medium (Control, C) or with DOX (5μM) for 24h, without or with the pan-NADPH oxidase inhibitor, VAS2870, at a range of concentrations (VAS 10, 50 and 100μM). Fluorescent readout of (A) cell viability (AFC) and (B) cytotoxicity (R110). (C) Caspase-Glo 3/7 assay of caspase 3/7 activity (DEVD). Data (Control □, DOX ■) are shown as mean value (±SEM) (n=6 experiments, 3-4 replicates in each which were averaged to provide a single value) and analyses performed using a two-factor ANOVA followed by paired Student's t-test or Dunnett's test. *P<0.05 vs respective No DOX; #P<0.05 vs respective no VAS (Control). RLU, relative light units.

TABLE 1

	WT Control	WT DOX	Nox2$^{-/-}$ Control	Nox2$^{-/-}$ DOX
HR (bpm)	429 ± 10 (23)	449 ± 17 (24)	406 ± 13 (23)	436 ± 23 (29)
IVSD (mm)	0.80 ± 0.02 (23)	0.78 ± 0.02 (24)	0.84 ± 0.03 (23)	0.77 ± 0.02 (29)
IVSS (mm)	1.18 ± 0.06 (23)	1.13 ± 0.07 (24)	1.18 ± 0.15 (23)	1.16 ± 0.06 (29)
LVPWD (mm)	0.81 ± 0.03 (23)	0.79 ± 0.04 (24)	0.76 ± 0.02 (23)	0.94 ± 0.06 (29)
LVPWS (mm)	1.13 ± 0.07 (23)	1.07 ± 0.05 (24)	1.08 ± 0.07 (23)	1.28 ± 0.06 (29)
LVEDD (mm)	4.21 ± 0.05 (23)	4.21 ± 0.05 (24)	4.15 ± 0.06 (23)	4.06 ± 0.05 (29)
LVESD (mm)	2.91 ± 0.08 (23)	2.92 ± 0.07 (24)	3.02 ± 0.08 (23)	2.77 ± 0.08 (29)
Fractional shortening (%)	30.50 ± 1.42 (10)	26.06 ± 0.93* (16)	30.27 ± 1.67 (10)	28.91 ± 0.85 (17)
MV E/A	1.76 ± 0.07 (19)	1.44 ± 0.05* (17)	1.53 ± 0.10 (17)	1.63 ± 0.08 (25)
TL (mm)	18.36 ± 0.28 (19)	18.39 ± 0.28 (17)	18.32 ± 0.29 (22)	18.06 ± 0.22 (23)
LV/TL (mg/mm)	6.01 ± 0.30 (19)	5.14 ± 0.18* (17)	6.08 ± 0.18 (22)	5.73 ± 0.16 (23)
LV cardiomyocyte cross-sectional area (μm^2)	455.7 ± 25.6 (5)	347.5 ± 7.0* (5)	386.6 ± 1.3 (5)	394.7 ± 10.4 (5)

Effects of doxorubicin on cardiac structure and function: Electrocardiographic measurements were taken from short axis M-mode recordings (HR, heart rate; IVSD, interventricular septal thickness in diastole; IVSS, interventricular septal thickness in systole; LVPWD, left ventricular posterior wall thickness in diastole; LVPWS, left ventricular posterior wall thickness in systole; LVEDD, left ventricular end-diastolic diameter; LVESD, left ventricular end-systolic diameter), and mitral valve (MV) E/A ratio assessed by pulse-wave Doppler flow. LV mass/tibial length (TL) ratio was assessed and myocyte cross-sectional area measured after haematoxylin and eosin staining. Data are shown as mean±SEM (n, number of animals) and analysis performed by two-factor ANOVA, followed by unpaired Student's t-test, as indicated. *P<0.05 vs WT Control.

Figure 1

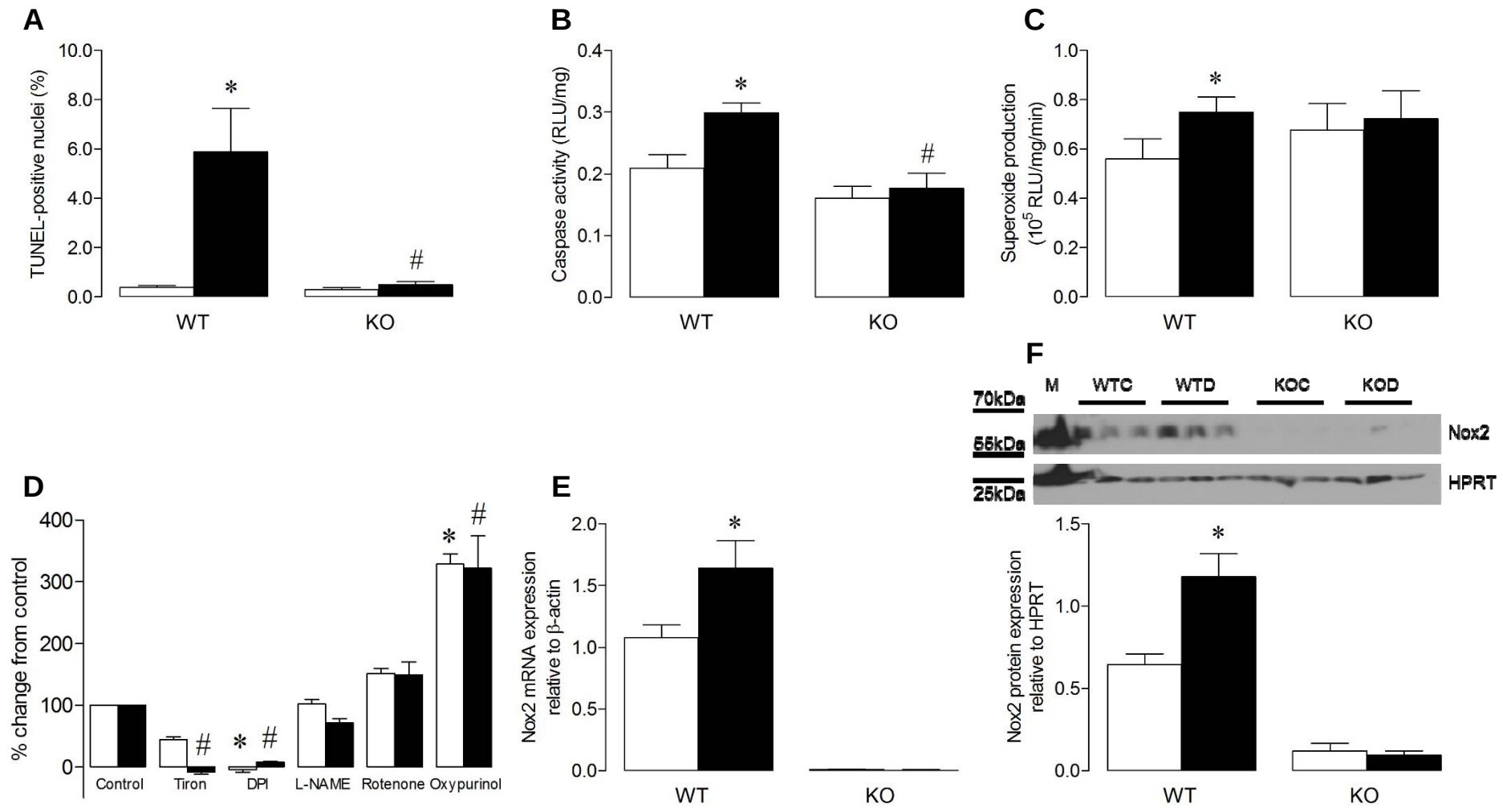
A
TUNEL-positive nuclei (%)
10.0
8.0
6.0
4.0
2.0
0.0
*
#
WT
KO
B
Caspase activity (RLU/mg)
0.4
0.3
0.2
0.1
0.0
*
#
WT
KO
C
Superoxide production
(10^5 RLU/mg/min)
1.0
0.8
0.6
0.4
0.2
0.0
*
WT
KO
D
% change from control
400
300
200
100
0
#
* #
* #
Control
Tiron
DPI
L-NAME
Rotenone
Oxypurinol
E
Nox2 mRNA expression
relative to β-actin
2.0
1.5
1.0
0.5
0.0
*
WT
KO
F
M
WTC
WTD
KOC
KOD
70kDa
55kDa
25kDa
Nox2
HPRT
Nox2 protein expression
relative to HPRT
1.5
1.0
0.5
0.0
*
WT
KO

Figure 2

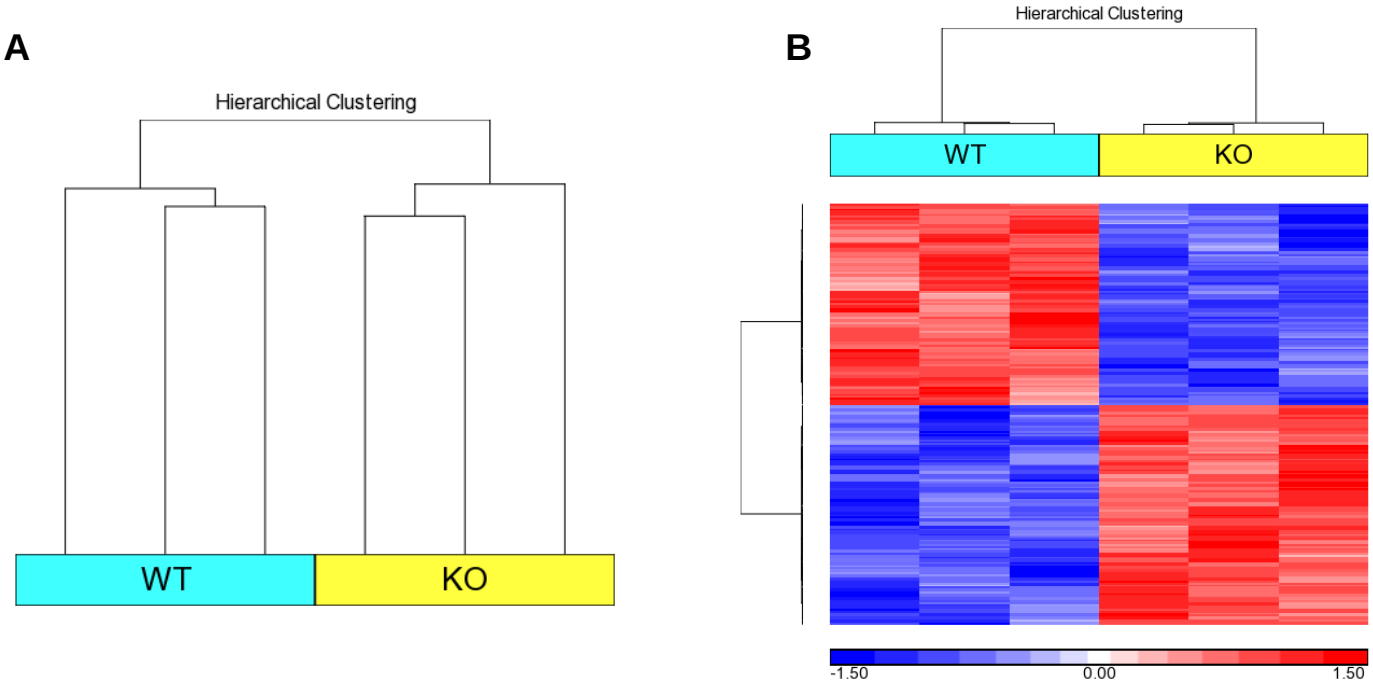
A
Hierarchical Clustering
WT
KO
B
Hierarchical Clustering
WT
KO
-1.50
0.00
1.50
C
ID
KO
WT
PCA Mapping (67.8%)
PC #2 22.6%
PC #1 27.2%
D
Sources of Variation
Mean F Ratio
3.5
2.8
2.1
1.4
0.7
0.0
3.45
1.00
ID
Error
Factors

Figure 3

The analysis is composed of 12 networks. To view a network, select the appropriate network(s) and click View Networks. To merge selected networks, click Merge Networks. Total selected molecules: 35

ID	Molecules in Network	Score	Focus Molecules	Top Functions
1	↑**ALAS1,** Calcineurin protein(s), ↓**CCL21*,** CD3, ↑**CD63,** ↓**CD74,** ↓**CD8B,** cytochrome C, ↓**DBP,** ↑**EHD4,** ↓**GOLGB1,** ↑**H2AFY,** HLA-DR, ↓**HLA-DRB1,** ↓**IGFBP6,** ↑**LUC7L3,** MAP2K1/2, ↑**MEF2C,** Nfat (family), NFkB (complex), Notch, ↓**PER2,** ↑**PHLDA1,** ↑**PLIN2,** ↑**PPARGC1A,** ↑**PPARGC1B,** ↑**PTP4A2,** ↓**PVALB,** ↑**Rcan2,** Rxr, ↓**SERPINF1,** ↑**SLC25A20,** ↑**VMP1,** ↑**VTI1B*,** ↑**ZC3H13**	47	26	Lipid Metabolism, Molecular Transport, Small Molecule Biochemistry
2	↑**BCL2L13,** caspase, ↓**CYP27A1,** ↑**DYNLL2,** ↑**ERH,** ERK, Focal adhesion kinase, ↓**GLS,** ↑**GNA13,** ↑**HBB,** ↑**HBD,** hemoglobin, HISTONE, ↓**HLA-DQB1*,** ↑**HNRNPA2B1,** ↑**HNRNPH1*,** HSP, ↑**HSPA8,** ↑**HSPB3,** ↑**HSPD1,** IgG, IL12 (complex), Immunoglobulin, ↑**INSIG2,** Interferon alpha, MHC Class II (complex), ↑**NIPBL,** p85 (pik3r), PI3K (complex), ↑**PRMT1,** ↑**SBDS,** Sos, ↑**SRPX,** ↑**SUMO3*,** TCR	37	20	Hematological System Development and Function, Molecular Transport, Small Molecule Biochemistry
3	↑**ACTA2*,** ↑**ACTB,** Actin, ↓**AGRN,** ↑**AHSA1,** Alpha Actinin, Alpha catenin, Alpha tubulin, Collagen type IV, Collagen(s), ↑**DAG1,** ↓**DKK3,** Dynamin, dystroglycan, ERK1/2, F Actin, Fibrin, G-Actin, Hsp90, ↑**HSPB1,** ↓**INPPL1,** Laminin, ↓**MDK,** ↑**MFN2,** ↑**NDRG2,** ↑**PDPK1,** ↓**PLD1,** PP2A, ↑**RABL6,** ↑**SYNM,** ↑**TUBA8,** ↑**TUBB6,** ↑**TUBB4B,** Tubulin, Ubiquitin	31	18	Cellular Assembly and Organization, Cellular Function and Maintenance, Cell Death and Survival
4	Akt, Alp, ↓**ANGPTL7,** ↓**ANKH,** Ap1, ↑**CCND2*,** ↓**CDH5,** Cg, Collagen type I, Creb, estrogen receptor, ↑**FOXN3,** FSH, ↓**GDF10,** ↑**HDLBP,** Hsp27, Igm, Ikb, IL1, LDL, ↓**LY6E,** ↑**MAT2A*,** ↓**MMP2,** Mmp, P38 MAPK, Pdgf (complex), PDGF BB, Pld, ↑**SNURF,** ↓**SPARC,** Tgf beta, ↓**TGFBR3,** ↓**TIMP3,** ↑**TRA2B,** ↓**VAPB**	28	16	Cancer, Renal and Urological Disease, Cardiovascular System Development and Function
5	ADH1C, ↓**ANKRD12,** APP, ↓**C1orf51,** ↓**C2orf40,** ↑**CACNA2D1,** CACNB1, CACNG5, CCND1, CXCL12, CYP2D6, ↑**DDX24,** ↓**EPHX1,** ethanol, ↑**FAM134B,** GSPT2, ↓**INMT*,** LIMCH1, ↓**MDK,** MGST3, MIR17HG, ↑**MLF2,** NAT2, ↑**NDUFAF4*,** ↑**NMRK2,** ↑**OPA3,** ↓**PAPSS2,** RLBP1, ROR1, ↓**SAMD9L,** SULF2, TPI1, TRDMT1, tretinoin, ↑**TUBB6**	27	16	Lipid Metabolism, Small Molecule Biochemistry, Vitamin and Mineral Metabolism
6	↓**ABCA9,** ↑**ANP32E,** ↓**BDH2,** C5orf44, ↑**CALU,** CEP192, CTNNAL1, FYTTD1, GGCX, HLTF, IKZF1, ↓**ITPRIPL1,** ↑**KIAA1551,** KRT79, ↓**MID1IP1,** PAPSS1, ↓**PAPSS2,** ↑**PROSC,** ↓**SCARA3,** SULF2, TNPO2, ↑**TNPO3,** TRAPPC1, ↑**TRAPPC3,** TRAPPC4, TRAPPC5, TRAPPC8, TRAPPC9, TRAPPC11, TRAPPC2L, TRAPPC6B, ↑**TSPAN3,** UBC, ↑**ZFP91,** ↑**ZNF445**	26	15	Connective Tissue Disorders, Developmental Disorder, Hereditary Disorder
7	ACTA1, ↑**ADSSL1,** ARHGAP27, ARID5B, ↓**C16orf72,** CASKIN2, COPS5, CTNNB1, ELAVL1, FOXN2, ↑**GKAP1,** ↑**GNB5,** HGS, ↓**ITGBL1,** KIAA1522, ↓**LARS,** ↑**LDB3*,** LEMD2, MAP7D3, ↓**PALD1,** PHACTR4, ↑**PRPF19,** SAMD1, ↑**SH3KBP1*,** SLAIN2, SRF, SYDE1, ↑**TBX20,** TGFB1, ↑**TMEM63B,** ↑**TNNI3K,** UBC, ↓**WDFY1,** YWHAZ, ZFP161	23	14	Embryonic Development, Organ Development, Organismal Development
8	AMPK, AQP4, ↓**BRD2,** CD93, Ck2, ↓**DBP,** EPHA4, hemin, Histone h3, Histone h4, Il8r, Insulin, Jnk, KAT6B, Lh, Mapk, MIR17HG, MST1R, ↓**PER2,** ↑**PFKM,** ↑**PHLDA1,** Pkc(s), ↑**PPM1L,** Rac, RAPGEF3, Ras, Ras homolog, RNA polymerase II, S1PR2, S1PR3, SESN2, SLC6A2, ↓**SMARCC2,** SMPD1, Vegf	9	7	Organismal Development, Cell Death and Survival, Cellular Compromise
9	APCS, APOA4, APOC2, BCKDHA, BTG1, CD34, CIDEC, CLTCL1, CRY1, DBT, GSPT1, Hamp/Hamp2, HNF4A, HNRNPA0, IL10RA, LTB4R2, ↑**MTF2,** NFE2L1, PCK2, ↑**PEX11A*,** PEX11B, pyruvaldehyde, RNASE4, SELE, SKI, Slco1a4, ST13, ↑**ST6GALNAC6,** SULT2A1, TIA1, TNF, ↑**UQCC,** ↑**VMP1,** WTAP, ↓**YPEL3**	8	6	Developmental Disorder, Hereditary Disorder, Metabolic Disease
10	↓**Ahnak2,** GH1	2	1	Cancer, Cell Cycle, Cell Morphology
11	↓**MMRN2,** VDR	2	1	Cardiovascular Disease, Cell Morphology, Cellular Development
12	↑**LRTM1*,** RORA, RORC	2	1	Cellular Growth and Proliferation, Hematological System Development and Function, Tissue Development

Figure 4A

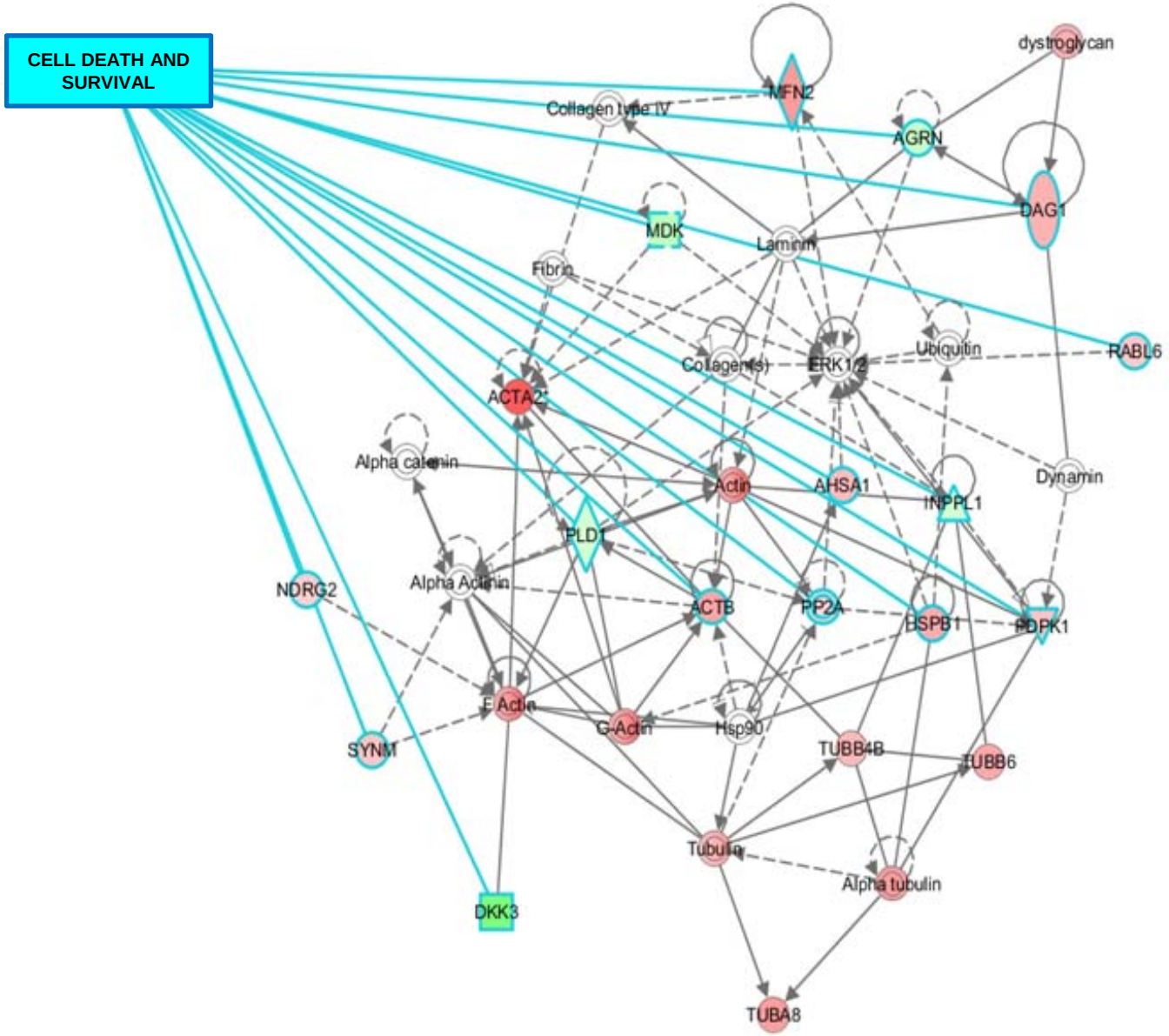
CELL DEATH AND SURVIVAL
dystroglycan
MFN2
Collagen type IV
AGRN
DAG1
MDK
Laminin
Fibrin
Ubiquitin
RABL6
Collagen(s)
ERK1/2
ACTA2
Alpha catenin
Actin
AHSA1
Dynamin
INPPL1
PLD1
NDRG2
Alpha Actinin
ACTB
PP2A
HSPB1
PDPK1
F Actin
G-Actin
Hsp90
SYNM
TUBB4B
TUBB6
Tubulin
Alpha tubulin
DKK3
TUBA8

Figure 4B

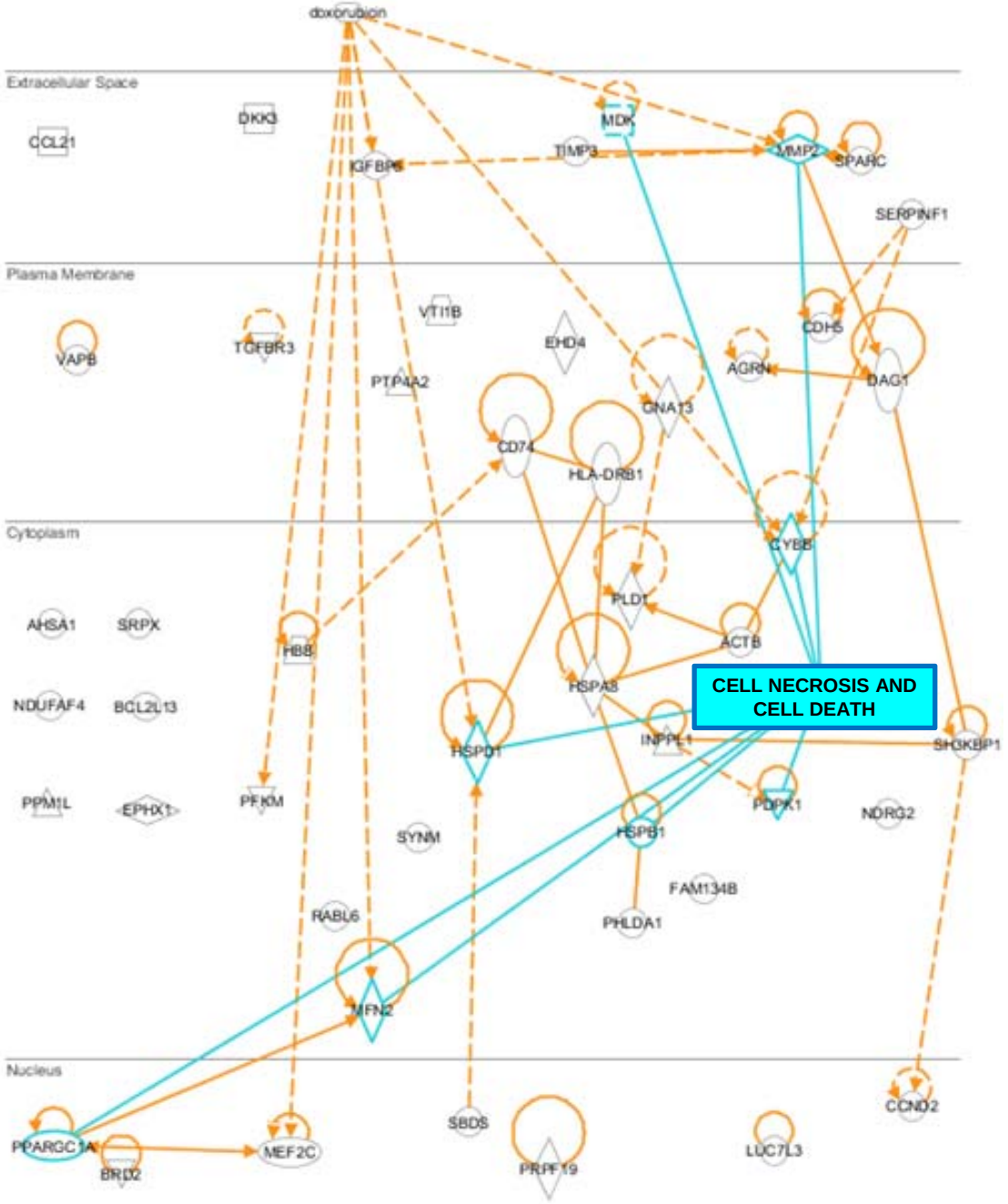
doxorubicin
Extracellular Space
DKK3
CCL21
IGFBP6
MDK
TIMP3
MMP2
SPARC
SERPINF1
Plasma Membrane
VTI1B
TGFBR3
VAPB
EHD4
PTP4A2
GNA13
AGRN
CDH5
DAG1
CD74
HLA-DRB1
GYPB
Cytoplasm
PLD1
AHSA1
SRPX
HBB
ACTB
HSPA8
CELL NECROSIS AND CELL DEATH
NDUFAF4
BCL2L13
HSPD1
INPPL1
SH3KBP1
PPM1L
EPHX1
PFKM
PDPK1
NDRG2
SYNM
HSPB1
FAM134B
RABL6
PHLDA1
MFN2
Nucleus
CCND2
SBDS
PPARGC1A
MEF2C
BRD2
PRPF19
LUC7L3

Figure 5

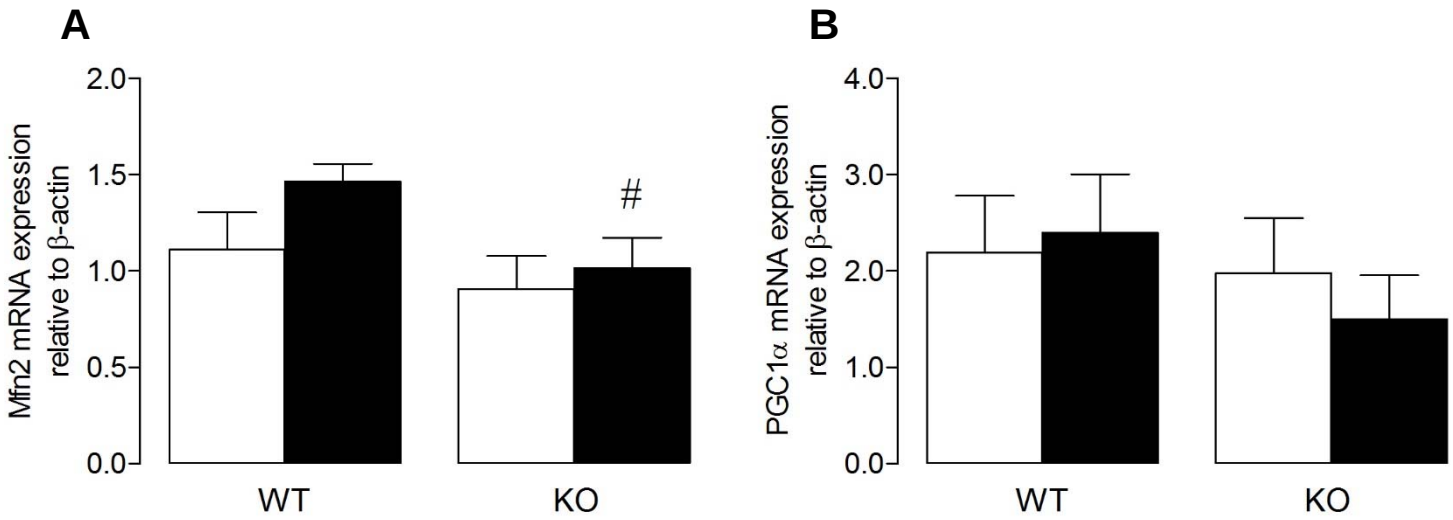
A
Mfn2 mRNA expression relative to β-actin
2.0
1.5
1.0
0.5
0.0
#
WT
KO
B
PGC1α mRNA expression relative to β-actin
4.0
3.0
2.0
1.0
0.0
WT
KO

Figure 6

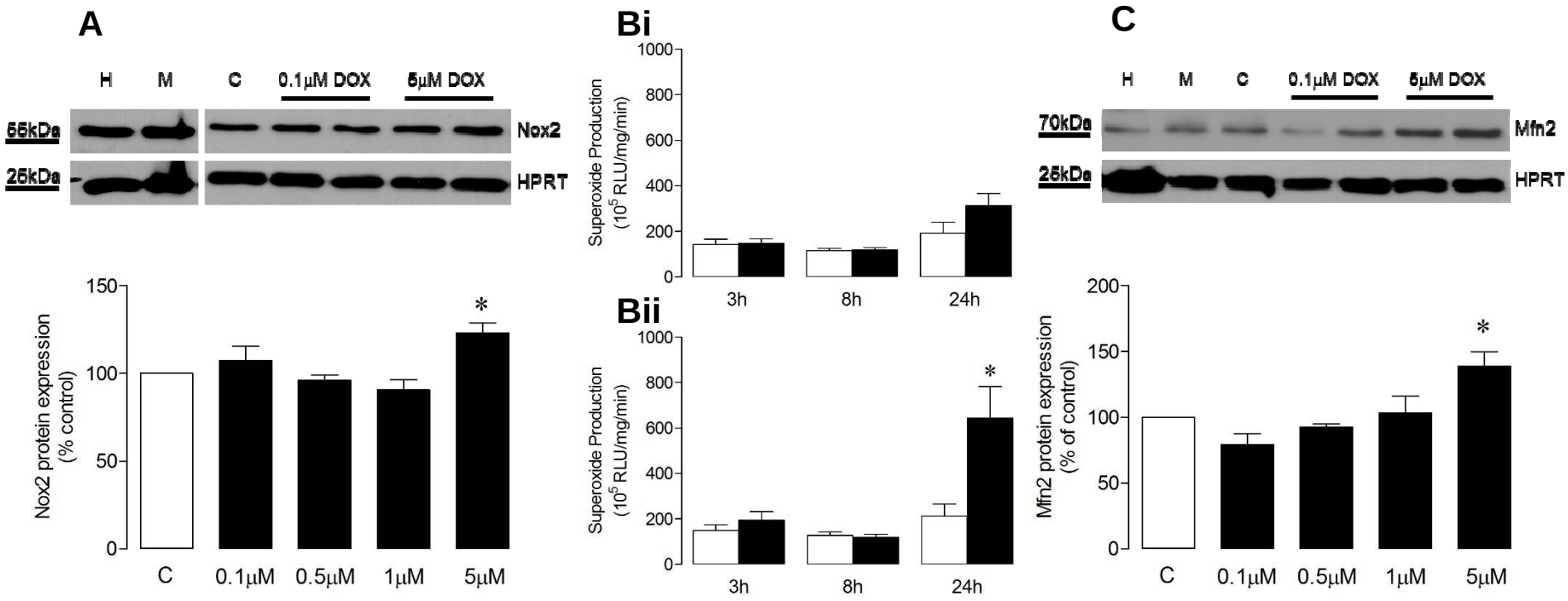
A
H
M
C
0.1μM DOX
5μM DOX
55kDa
Nox2
25kDa
HPRT
Nox2 protein expression (% control)
150
100
50
0
*
C
0.1μM
0.5μM
1μM
5μM
Bi
Superoxide Production (10^5 RLU/mg/min)
1000
800
600
400
200
0
3h
8h
24h
Bii
Superoxide Production (10^5 RLU/mg/min)
1000
800
600
400
200
0
*
3h
8h
24h
C
H
M
C
0.1μM DOX
5μM DOX
70kDa
Mfn2
25kDa
HPRT
Mfn2 protein expression (% of control)
200
150
100
50
0
*
C
0.1μM
0.5μM
1μM
5μM

Figure 7

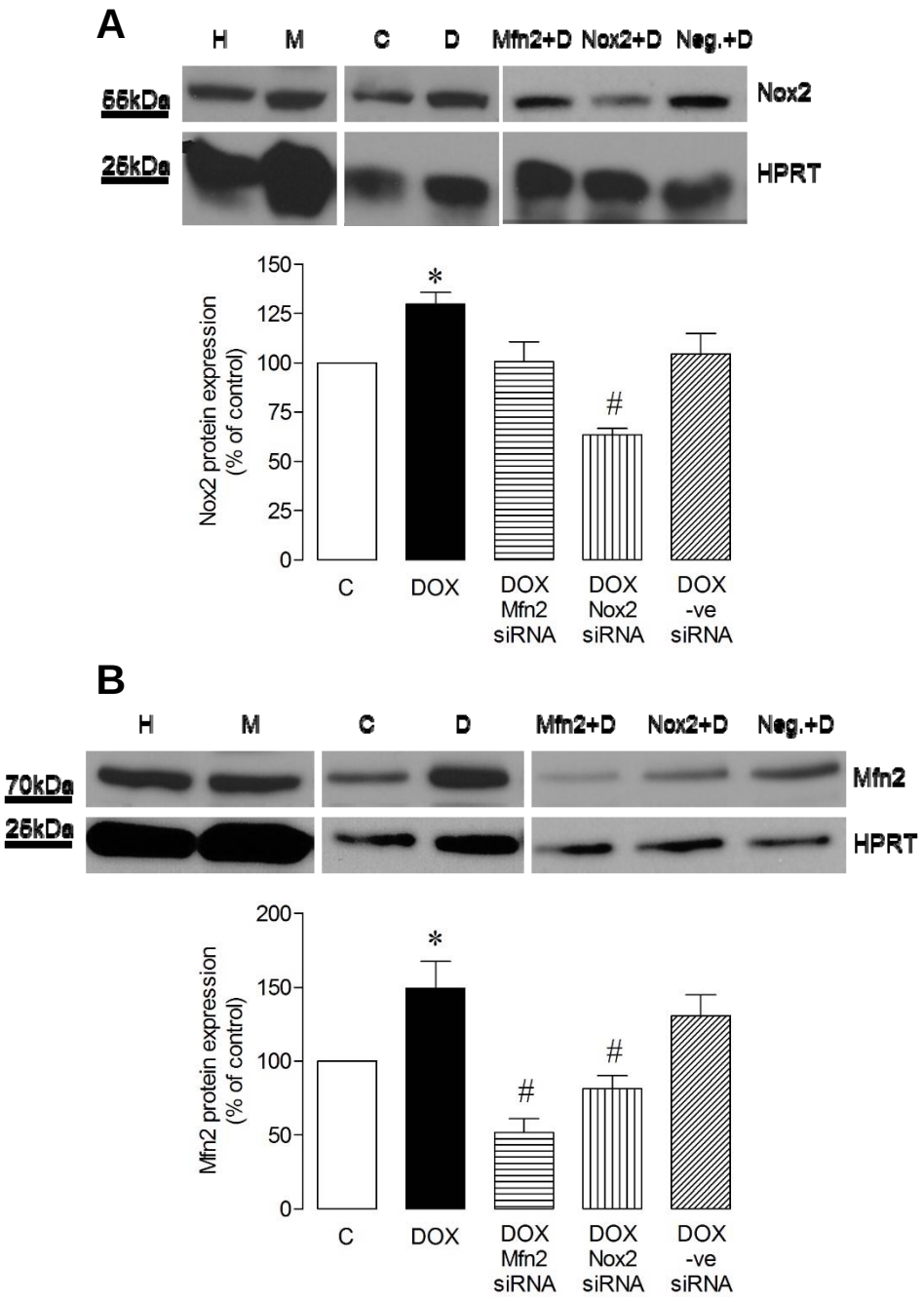
A
H
M
C
D
Mfn2+D
Nox2+D
Neg.+D
55kDa
Nox2
25kDa
HPRT
Nox2 protein expression (% of control)
150
125
100
75
50
25
0
*
#
C
DOX
DOX Mfn2 siRNA
DOX Nox2 siRNA
DOX -ve siRNA
B
H
M
C
D
Mfn2+D
Nox2+D
Neg.+D
70kDa
Mfn2
25kDa
HPRT
Mfn2 protein expression (% of control)
200
150
100
50
0
*
#
#
C
DOX
DOX Mfn2 siRNA
DOX Nox2 siRNA
DOX -ve siRNA

Figure 8

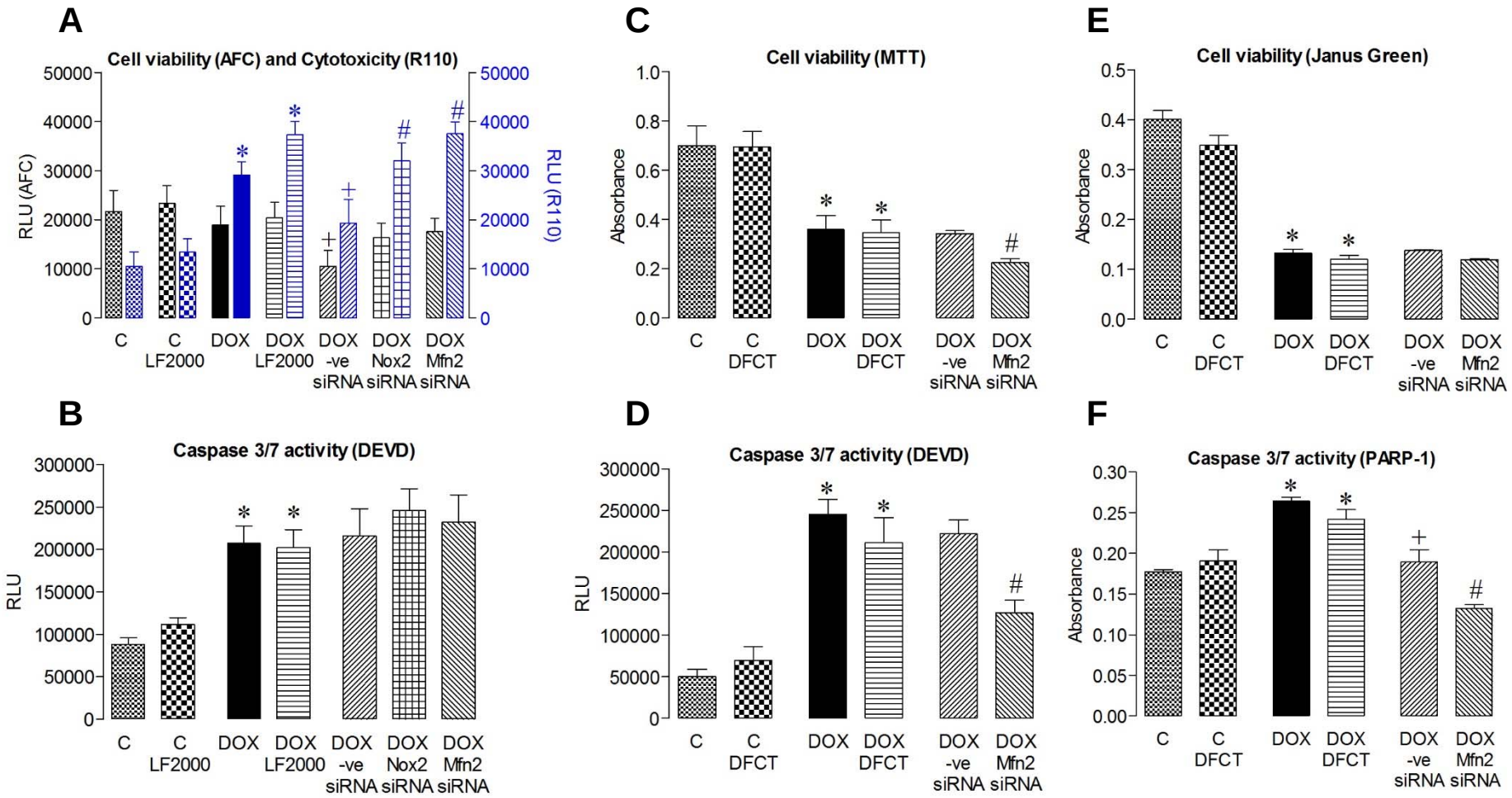
A
Cell viability (AFC) and Cytotoxicity (R110)
RLU (AFC)
RLU (R110)
50000
40000
30000
20000
10000
0
C
C LF2000
DOX
DOX LF2000
DOX -ve siRNA
DOX Nox2 siRNA
DOX Mfn2 siRNA
B
Caspase 3/7 activity (DEVD)
RLU
300000
250000
200000
150000
100000
50000
0
C
C LF2000
DOX
DOX LF2000
DOX -ve siRNA
DOX Nox2 siRNA
DOX Mfn2 siRNA
C
Cell viability (MTT)
Absorbance
1.0
0.8
0.6
0.4
0.2
0.0
C
C DFCT
DOX
DOX DFCT
DOX -ve siRNA
DOX Mfn2 siRNA
D
Caspase 3/7 activity (DEVD)
RLU
300000
250000
200000
150000
100000
50000
0
C
C DFCT
DOX
DOX DFCT
DOX -ve siRNA
DOX Mfn2 siRNA
E
Cell viability (Janus Green)
Absorbance
0.5
0.4
0.3
0.2
0.1
0.0
C
C DFCT
DOX
DOX DFCT
DOX -ve siRNA
DOX Mfn2 siRNA
F
Caspase 3/7 activity (PARP-1)
Absorbance
0.30
0.25
0.20
0.15
0.10
0.05
0.00
C
C DFCT
DOX
DOX DFCT
DOX -ve siRNA
DOX Mfn2 siRNA

Figure 9

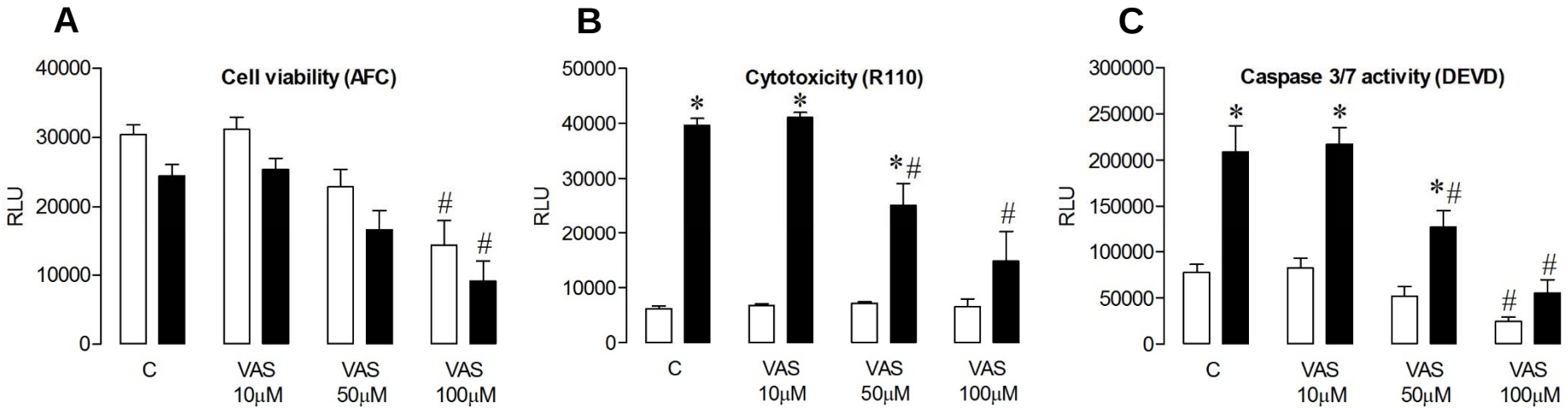
A
Cell viability (AFC)
RLU
40000
30000
20000
10000
0
C
VAS 10μM
VAS 50μM
VAS 100μM
#
B
Cytotoxicity (R110)
50000
40000
30000
20000
10000
0
*
*#
C
Caspase 3/7 activity (DEVD)
300000
250000
200000
150000
100000
50000

SUPPORTING INFORMATION

SIGNALLING MECHANISMS UNDERLYING DOXORUBICIN AND NOX2 NADPH OXIDASE-INDUCED CARDIOMYOPATHY: INVOLVEMENT OF MITOFUSIN-2

Declan McLaughlin[1], Youyou Zhao[1], Karla M. O'Neill[1], Kevin S. Edgar[1], Philip D. Dunne[2], Anna M. Kearney[1], David J. Grieve[1], Barbara J. McDermott[1]

Queen's University Belfast, [1]Wellcome-Wolfson Institute for Experimental Medicine, and [2]Centre for Cancer Research & Cell Biology, Belfast BT9 7AE, UK

TABLE S1: Real-time RT-PCR primer sequences

Gene	Forward Sequence	Reverse Sequence
β-actin	5' CGT GAA AAG ATG ACC CAG ATC A 3'	5' TGG TAC GAC CAG AGG CAT ACA G 3'
Nox2	5' ACT CCT TGG GTC AGC ACT GG 3'	5' GTT CCT GTC CAG TTG TCT TCG 3'
GPx1	5' AGG CTC ACC CGC TCT TTA CC 3'	5' GGG TCG TCA CTG GGT GTT G 3'
NOS1 (nNOS)	5' GAC TGA TGG CAA GCA TGA CTT C 3'	5' GCC CAA GGT AGA GCC ATC TG 3'
NOS2 (iNOS)	5' TGA CGG CAA ACA TGA CTT CAG 3'	5' GCC ATC GGG CAT CTG GTA 3'
NOS3 (eNOS)	5' TCT GCG GCG ATG TCA CTA TG 3'	5' CCA TGC CGC CCT CTG TT 3'
SOD1	5' AGC ATT CCA TCA TTG GCC GTA 3'	5' TTT CCA CCT TTG CCC AAG TCA 3'
SOD2	5' ACA GAT TGC TGC CTG CTC TAA TCA 3'	5' TAA GCG TGC TCC CAC ACG TC 3'
Glutaredoxin1	5' CCC TTC CCA CTC CTG CAT T 3'	5' GGA GGT TGA GGC TGA GAA CAC T 3'
Glutaredoxin2	5' TTT GTC AAT GGA CGA TTT ATT GGA 3'	5'GCA GCA ATT TCC CTT CTT TGT G 3'
Catalase	5' TTC AGA AGA AAG CGG TCA AGA AT 3'	5' GAT GCG GGC CCC ATA GTC 3'
Peroxisome proliferator-activated receptor gamma coactivator 1-alpha (PGC-1α)	5' CAG CCC AGA GTC ACC AAA TGA 3'	5' TTC CAG AGA GTT CCA CAC TTA AGG T 3'
Mitofusin 2 (Mfn2)	5' CAG TTG GTG TCT GGC ATT GTG 3'	5' AGG GCC TCA GTG GCA AGA A 3'

Real-time RT-PCR primer sequences were generated using Primer Express Software (Applied Biosystems, UK) and primers obtained from Invitrogen (UK).

TABLE S2: Differentially expressed genes in LV tissue from WT vs. Nox$^{-/-}$ mice

(A) Upregulated genes

DEFINITION	Gene ID	logFC	Ave Expr	p value	Adj. p value
integrin beta 1 binding protein 3 (Itgb1bp3)	ITGB1BP3	1.169	7.96	7.31E-04	0.093
hemoglobin, beta adult major chain (Hbb-b1)	HBB-B1	0.973	9.32	1.77E-04	0.049
actin, alpha 2, smoothcle, aorta (Acta2)	ACTA2	0.783	9.56	3.57E-08	0.001
pleckstrin homology-like domain, family A, member 1 (Phlda1)	PHLDA1	0.695	9.26	3.36E-05	0.028
DEAD (Asp-Glu-Ala-Asp) box polypeptide 24 (Ddx24)	DDX24	0.627	8.57	8.66E-06	0.016
heterogeneous nuclear ribonucleoprotein A2/B1 (Hnrnpa2b1), transcript variant 2	HNRNPA2B1	0.615	9.54	4.05E-05	0.028
RIKEN cDNA 1810015C04 gene (1810015C04Rik), transcript variant 2	1810015C04RIK	0.588	11.31	2.73E-04	0.063
PREDICTED: similar to mitofusin 2, transcript variant 1 (LOC100044767)	MFN2	0.573	8.06	1.73E-04	0.048
phosphofructokinase,cle (Pfkm)	PFKM	0.562	8.82	3.26E-04	0.068
tubulin, alpha 8 (Tuba8)	TUBA8	0.548	9.49	9.23E-05	0.039
SH3-domain kinase binding protein 1 (Sh3kbp1)	SH3KBP1	0.543	9.96	2.37E-06	0.010
	HRMT1L2	0.518	9.31	8.79E-04	0.096
heat shock protein 1 (chaperonin) (Hspd1)	HSPD1	0.516	9.87	5.78E-06	0.012
cyclin D2 (Ccnd2)	CCND2	0.512	9.60	1.88E-05	0.024
actin, beta, cytoplasmic (Actb)	ACTB	0.509	8.58	9.59E-04	0.099
PREDICTED: similar to human protein homologous to DROER protein (LOC100042777)	LOC100042777	0.503	8.89	5.49E-05	0.034
peroxisome proliferative activated receptor, gamma, coactivator 1 alpha (Ppargc1a)	PPARGC1A	0.500	8.92	3.58E-06	0.010
trafficking protein particle complex 3 (Trappc3)	TRAPPC3	0.500	8.34	4.08E-05	0.028
Nipped-B homolog (Drosophila) (Nipbl), transcript variant A	NIPBL	0.489	8.58	1.73E-05	0.024
tubulin, beta 6 (Tubb6)	TUBB6	0.487	8.62	3.93E-04	0.076
transmembrane protein 63b (Tmem63b)	TMEM63B	0.473	9.59	4.19E-05	0.028
heat shock protein 1 (Hspb1)	HSPB1	0.471	9.84	1.97E-05	0.024
acidic (leucine-rich) nuclear phosphoprotein 32 family, member E (Anp32e)	ANP32E	0.468	9.10	1.12E-04	0.039
calcium channel, voltage-dependent, alpha2/delta subunit 1 (Cacna2d1)	CACNA2D1	0.467	8.77	2.92E-05	0.028
dystroglycan 1 (Dag1)	DAG1	0.438	9.46	4.40E-04	0.078
peroxisomal biogenesis factor 11a (Pex11a)	PEX11A	0.433	8.13	3.29E-05	0.028
enhancer of rudimentary homolog (Drosophila) (Erh)	ERH	0.430	9.14	1.49E-04	0.045
RIKEN cDNA 3300001P08 gene (3300001P08Rik)	3300001P08RIK	0.423	9.93	3.48E-04	0.070
heat shock protein 8 (Hspa8)	HSPA8	0.410	10.63	6.99E-05	0.036
vesicle transport through interaction with t-SNAREs 1B homolog (Vti1b)	VTI1B	0.406	8.02	6.13E-04	0.087

	D630048P19RIK	0.396	8.60	2.67E-05	0.028
tubulin, beta 2c (Tubb2c)	TUBB2C	0.394	11.44	2.81E-04	0.063
methionine adenosyltransferase II, alpha (Mat2a)	MAT2A	0.388	8.11	1.42E-04	0.045
AHA1, activator of heat shock protein ATPase homolog 1 (yeast) (Ahsa1)	AHSA1	0.387	8.14	4.42E-04	0.078
protein tyrosine phosphatase 4a2 (Ptp4a2)	PTP4A2	0.384	8.12	1.87E-04	0.050
transportin 3 (Tnpo3)	TNPO3	0.372	8.32	2.79E-04	0.063
sushi-repeat-containing protein (Srpx)	SRPX	0.371	7.08	6.37E-04	0.087
forkhead box N3 (Foxn3)	FOXN3	0.370	8.81	3.19E-04	0.067
	3000003G13RIK	0.369	9.18	2.15E-04	0.055
solute carrier family 25 (mitochondrial carnitine/acylcarnitine translocase), member 20 (Slc25a20)	SLC25A20	0.368	8.85	1.00E-04	0.039
PREDICTED: predicted gene, EG433144 (EG433144)	EG433144	0.364	9.15	2.61E-04	0.061
guanine nucleotide binding protein (G protein), beta 5 (Gnb5), transcript variant 1	GNB5	0.354	8.13	1.24E-04	0.040
RIKEN cDNA 2410003P15 gene (2410003P15Rik)	2410003P15RIK	0.353	9.32	1.53E-04	0.045
aminolevulinic acid synthase 1 (Alas1)	ALAS1	0.352	12.39	3.96E-05	0.028
LIM domain binding 3 (Ldb3), transcript variant 6	LDB3	0.351	10.09	6.45E-05	0.036
peroxisome proliferative activated receptor, gamma, coactivator 1 beta (Ppargc1b)	PPARGC1B	0.351	9.58	7.38E-04	0.093
leucine-rich repeats and transmembrane domains 1 (Lrtm1)	LRTM1	0.349	9.86	6.77E-05	0.036
G kinase anchoring protein 1 (Gkap1)	GKAP1	0.347	8.57	4.48E-04	0.079
TNNI3 interacting kinase (Tnni3k)	TNNI3K	0.344	8.26	7.64E-05	0.036
high density lipoprotein (HDL) binding protein (Hdlbp)	HDLBP	0.339	8.37	2.57E-04	0.061
heterogeneous nuclear ribonucleoprotein H1 (Hnrph1)	HNRPH1	0.338	9.43	6.20E-04	0.087
desmuslin (Dmn), transcript variant 3	DMN	0.336	7.36	4.23E-04	0.078
3-phosphoinositide dependent protein kinase-1 (Pdpk1), transcript variant 2	PDPK1	0.334	7.99	3.40E-04	0.070
BCL2-like 13 (apoptosis facilitator) (Bcl2l13), nuclear gene encoding mitochondrial protein	BCL2L13	0.331	8.21	5.08E-04	0.081
RIKEN cDNA 2810474O19 gene (2810474O19Rik)	2810474O19RIK	0.327	7.44	7.54E-05	0.036
proline synthetase co-transcribed (Prosc), transcript variant 3	PROSC	0.319	8.19	2.57E-04	0.061
regulator of calcineurin 2 (Rcan2), transcript variant 1	RCAN2	0.318	9.53	1.15E-04	0.039
RIKEN cDNA B230208H17 gene (B230208H17Rik) XM_897418 XM_897429 XM_897439 XM_897452 XM_897459 XM_914394 XM_923230 XM_923233 XM_923237 XM_923239 XM_923241 XM_923243 XM_923244 XM_923249 XM_923252	B230208H17RIK	0.306	7.85	5.54E-04	0.085
SNRPN upstream reading frame (Snurf)	SNURF	0.306	10.46	8.73E-04	0.096
	GNA13	0.306	8.17	8.88E-04	0.096
SMT3 suppressor of mif two 3 homolog 3 (yeast) (Sumo3)	SUMO3	0.304	8.33	4.79E-04	0.081
insulin induced gene 2 (Insig2)	INSIG2	0.303	9.52	1.70E-04	0.048
zinc finger CCCH type containing 13 (Zc3h13)	ZC3H13	0.303	7.13	2.31E-04	0.057

	LOC331507	0.302	9.47	1.49E-04	0.045
RIKEN cDNA 1700113I22 gene (1700113I22Rik)	1700113I22RIK	0.301	9.25	1.21E-04	0.040
splicing factor, arginine/serine-rich 10 (transformer 2 homolog, Drosophila) (Sfrs10)	SFRS10	0.299	8.01	9.80E-04	0.099
EH-domain containing 4 (Ehd4)	EHD4	0.293	12.64	8.95E-04	0.096
Cd63 antigen (Cd63), transcript variant 2	CD63	0.289	8.70	5.64E-04	0.085
	LOC384888	0.288	7.60	8.30E-04	0.096
RIKEN cDNA 1110007M04 gene (1110007M04Rik)	1110007M04RIK	0.288	11.27	4.42E-04	0.078
PRP19/PSO4 pre-mRNA processing factor 19 homolog (S cerevisiae) (Prpf19)	PRPF19	0.288	8.83	7.08E-04	0.092
myocyte enhancer factor 2C (Mef2c)	MEF2C	0.287	9.39	9.84E-04	0.099
calumenin (Calu), transcript variant 2	CALU	0.286	7.45	8.81E-04	0.096
dynein light chain LC8-type 2 (Dynll2)	DYNLL2	0.285	7.25	4.04E-04	0.076
adipose differentiation related protein (Adfp)	ADFP	0.283	7.71	6.00E-04	0.087
transmembrane protein 49 (Tmem49)	TMEM49	0.278	8.53	9.87E-04	0.099
PREDICTED: similar to medium-chain acyl-CoA dehydrogenase (LOC333331), misc RNA	LOC333331	0.277	12.15	8.97E-04	0.096
PREDICTED: similar to mitochondrial ribosomal protein S5 (LOC667609), misc RNA	LOC667609	0.269	9.11	6.06E-04	0.087
N-myc downstream regulated gene 2 (Ndrg2)	NDRG2	0.268	9.41	9.85E-04	0.099
myeloid leukemia factor 2 (Mlf2)	MLF2	0.263	8.77	7.55E-04	0.095
zinc finger protein 91 (Zfp91)	ZFP91	0.258	7.71	4.37E-04	0.078
Shwachman-Bodian-Diamond syndrome homolog (human) (Sbds)	SBDS	0.256	9.67	3.43E-04	0.070
	C730026J16	0.256	9.02	4.14E-04	0.077
H2A histone family, member Y (H2afy)	H2AFY	0.251	8.31	5.59E-04	0.085
	SIAT7F	0.251	7.10	3.02E-04	0.065
protein phosphatase 1 (formerly 2C)-like (Ppm1l)	PPM1L	0.246	7.73	4.91E-04	0.081
T-box 20 (Tbx20), transcript variant 1	TBX20	0.245	7.27	7.90E-04	0.096
heat shock protein 3 (Hspb3)	HSPB3	0.237	8.78	4.97E-04	0.081
	ZFP445	0.235	7.28	4.77E-04	0.081
adenylosuccinate synthetase like 1 (Adssl1)	ADSSL1	0.229	7.84	9.43E-04	0.098
	MTF2	0.225	8.15	7.26E-04	0.093
tetraspanin 3 (Tspan3)	TSPAN3	0.215	11.15	8.90E-04	0.096

(B) Downregulated genes

DEFINITION	Gene ID	logFC	Ave Expr	p value	Adj. p value
D site albumin promoter binding protein (Dbp)	DBP	-1.203	10.84	7.01E-05	0.036
RIKEN cDNA 1500015O10 gene (1500015O10Rik)	1500015O10RIK	-0.853	7.45	1.57E-05	0.024
Indolethylamine N-methyltransferase (Inmt)	INMT	-0.792	8.87	4.04E-04	0.076
PREDICTED: similar to beta chemokine Exodus-2 (LOC100041504)	LOC100041504	-0.746	8.77	8.91E-04	0.096
Gene model 129, (NCBI) (Gm129)	GM129	-0.721	7.32	5.46E-04	0.084
Chemokine (C-C motif) ligand 21b (Ccl21b)	CCL21B	-0.715	9.60	1.05E-04	0.039
Dickkopf homolog 3 (Xenopus laevis) (Dkk3)	DKK3	-0.695	7.47	6.56E-04	0.088
Vesicle-associated membrane protein, associated protein B and C (Vapb)	VAPB	-0.663	8.22	3.57E-06	0.010
Tissue inhibitor of metalloproteinase 3 (Timp3)	TIMP3	-0.554	10.42	1.13E-04	0.039
Angiopoietin-like 7 (Angptl7)	ANGPTL7	-0.536	7.73	5.86E-05	0.035
Epoxide hydrolase 1, microsomal (Ephx1)	EPHX1	-0.466	9.59	5.59E-06	0.012
Period homolog 2 (Drosophila) (Per2)	PER2	-0.462	8.34	2.12E-04	0.055
Transmembrane protein 82 (Tmem82)	TMEM82	-0.461	7.94	3.03E-04	0.065
Histocompatibility 2, class II antigen E beta (H2-Eb1)	H2-EB1	-0.441	9.32	1.84E-04	0.050
cDNA sequence X99384 (X99384)	X99384	-0.428	8.33	4.18E-05	0.028
Histocompatibility 2, class II antigen A, beta 1 (H2-Ab1)	H2-AB1	-0.420	9.68	2.76E-05	0.028
Mid1 interacting protein 1 (gastrulation specific G12-like (zebrafish)) (Mid1ip1)	MID1IP1	-0.408	10.00	5.10E-04	0.081
Serine (or cysteine) peptidase inhibitor, clade F, member 1 (Serpinf1)	SERPINF1	-0.402	10.39	7.87E-05	0.036
Parvalbumin (Pvalb)	PVALB	-0.389	7.21	9.25E-06	0.016
CD74 antigen (invariant polypeptide of major histocompatibility complex, class II antigen-associated) (Cd74)	CD74	-0.384	9.69	7.90E-04	0.096
Scavenger receptor class A, member 3 (Scara3)	SCARA3	-0.380	7.57	1.61E-04	0.047
PREDICTED: similar to MHC class II antigen beta chain (LOC641240)	LOC641240	-0.373	9.06	3.70E-04	0.072
cDNA sequence BC028528 (BC028528)	BC028528	-0.363	8.85	9.21E-04	0.097
Growth differentiation factor 10 (Gdf10)	GDF10	-0.359	7.50	3.43E-05	0.028
3'-Phosphoadenosine 5'-phosphosulfate synthase 2 (Papss2)	PAPSS2	-0.355	8.29	2.19E-04	0.055
Yippee-like 3 (Drosophila) (Ypel3)	YPEL3	-0.354	11.52	1.46E-04	0.045
Midkine (Mdk), transcript variant 3	MDK	-0.340	7.59	1.04E-04	0.039
Leucyl-tRNA synthetase (Lars)	LARS	-0.335	8.78	8.56E-05	0.038
Cytochrome P450, family 27, subfamily a, polypeptide 1 (Cyp27a1)	CYP27A1	-0.331	8.75	6.08E-04	0.087
Multimerin 2 (Mmrn2)	MMRN2	-0.321	9.22	1.21E-04	0.040
Insulin-like growth factor binding protein 6 (Igfbp6)	IGFBP6	-0.304	7.68	6.99E-04	0.092
PREDICTED: similar to HLA-G protein (LOC674135), misc RNA	LOC674135	-0.293	8.70	4.65E-04	0.081

	WDFY1	-0.293	7.79	1.12E-04	0.039
Secreted acidic cysteine rich glycoprotein (Sparc)	SPARC	-0.291	10.67	6.25E-04	0.087
Aagrin (Agrn)	AGRN	-0.290	9.64	2.15E-04	0.055
PREDICTED: sterile alpha motif domain containing 9-like, transcript variant 1 (Samd9l)	SAMD9L	-0.289	9.22	9.77E-04	0.099
Bromodomain containing 2 (Brd2), transcript variant 1	BRD2	-0.287	9.14	8.57E-04	0.096
PREDICTED: glutaminase, transcript variant 3 (Gls)	GLS	-0.281	8.25	6.56E-04	0.088
Integrin, beta-like 1 (Itgbl1)	ITGBL1	-0.279	8.22	9.24E-04	0.097
	CCDC3	-0.279	7.29	8.99E-04	0.096
Transforming growth factor, beta receptor III (Tgfbr3)	TGFBR3	-0.277	8.32	3.20E-04	0.067
Progressive ankylosis (Ank)	ANK	-0.275	10.20	5.07E-04	0.081
	6330403M23RIK	-0.272	9.22	5.39E-04	0.084
PREDICTED: RIKEN cDNA 1810013L24 gene (1810013L24Rik)	1810013L24RIK	-0.270	8.36	5.13E-04	0.081
PREDICTED: golgi autoantigen, golgin subfamily b, macrogolgin 1, transcript variant 9 (Golgb1)	GOLGB1	-0.268	8.17	8.04E-04	0.096
Cadherin 5 (Cdh5)	CDH5	-0.265	7.98	7.67E-04	0.096
Matrix metallopeptidase 2 (Mmp2)	MMP2	-0.264	9.93	2.55E-04	0.061
	4930533K18RIK	-0.262	8.22	6.39E-04	0.087
	1110046J11RIK	-0.261	11.35	8.01E-04	0.096
Ankyrin repeat domain 12 (Ankrd12)	ANKRD12	-0.259	7.71	5.01E-04	0.081
ATP-binding cassette transporter sub-family A member 9 (Abca9)	ABCA9	-0.259	7.73	3.64E-04	0.072
	LOC98434	-0.253	8.58	5.76E-04	0.086
Lymphocyte antigen 6 complex, locus E (Ly6e)	LY6E	-0.252	8.68	8.70E-04	0.096
	CD8B	-0.249	9.21	9.16E-04	0.097
SWI/SNF related, matrix associated, actin dependent regulator of chromatin, subfamily c, member 2 (Smarcc2)	SMARCC2	-0.246	7.82	8.85E-04	0.096
Inositol polyphosphate phosphatase-like 1 (Inppl1)	INPPL1	-0.240	10.74	5.88E-04	0.087
AHNAK nucleoprotein 2 (Ahnak2)	AHNAK2	-0.239	7.73	6.19E-04	0.087
3-Hydroxybutyrate dehydrogenase, type 2 (Bdh2)	BDH2	-0.232	7.23	7.32E-04	0.093
	PLD1	-0.228	7.66	8.24E-04	0.096
	1700041B20RIK	-0.218	8.19	8.77E-04	0.096

FIGURE S1: Time course of contractile dysfunction in response to DOX treatment

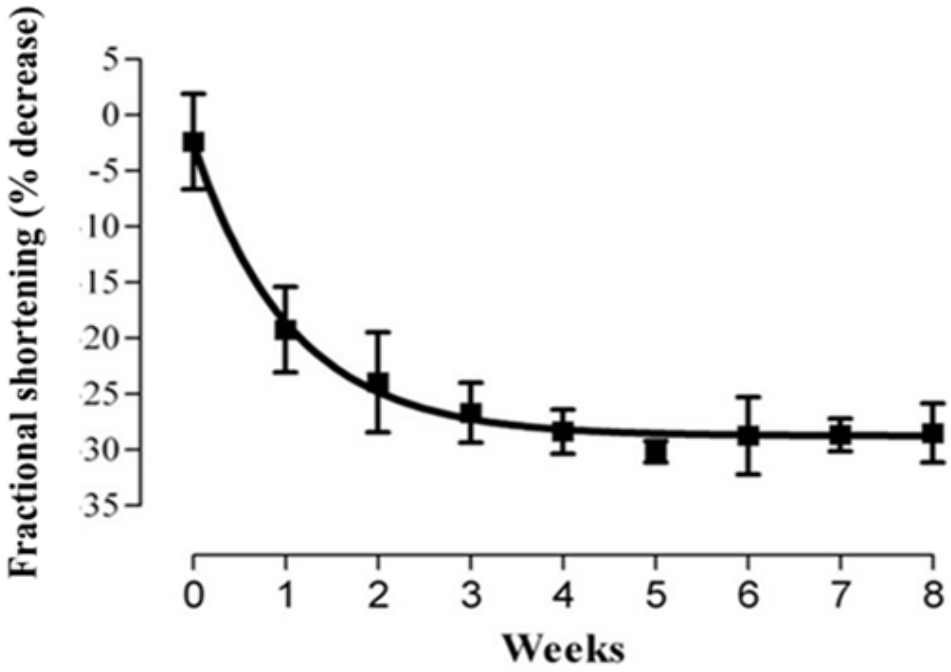

WT mice were administered saline or DOX (4mg/kg) by 3 weekly intraperitoneal (i.p.) injections and fractional shortening quantified at weekly intervals by echocardiography (n=9). Data are shown as mean±SEM and represent % decrease compared to WT control.

FIGURE S2: Effect of DOX on LV NOS isoenzyme and antioxidant gene mRNA expression

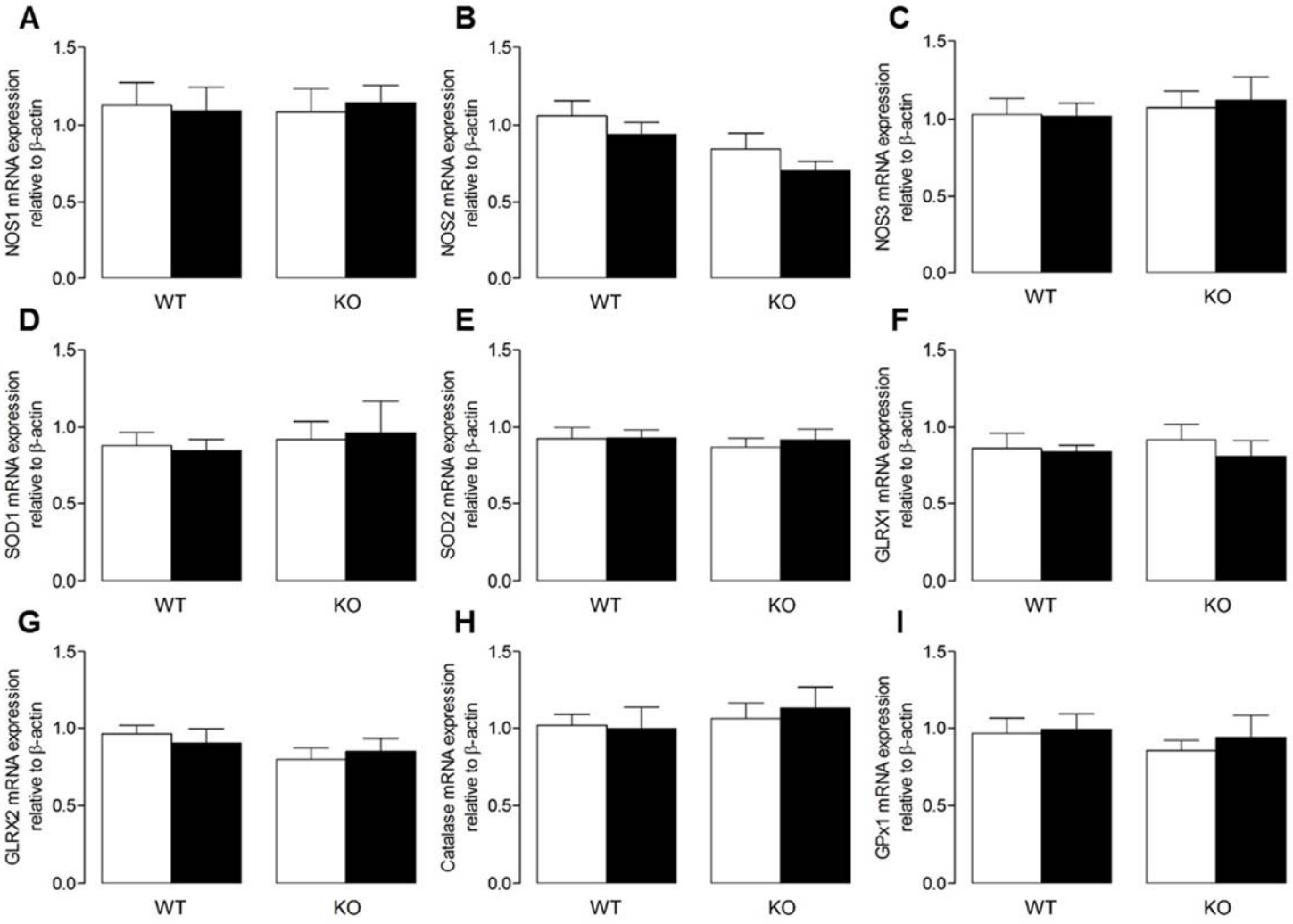

mRNA expression of (A) NOS1 (n=11-15), (B) NOS2 (n=12-13), (C) NOS3 (n=6-9), (D), superoxide dismutase 1 (SOD1, n=6-9), (E) SOD2 (n=7-9), (F), glutaredoxin 1 (GLRX1, n=6-8), (G) GLRX2 (n=11-13), (H) catalase (n=7-8), and (I) glutathione peroxidase (GPx1, n=10-13) by real-time RT-PCR. Data (Control □, DOX ■) are shown as mean (±SEM) and analyses performed using a two-factor ANOVA. P=NS.

FIGURE S3: Quality control assessment of Illumina MouseWG-6 v2.0 microarray

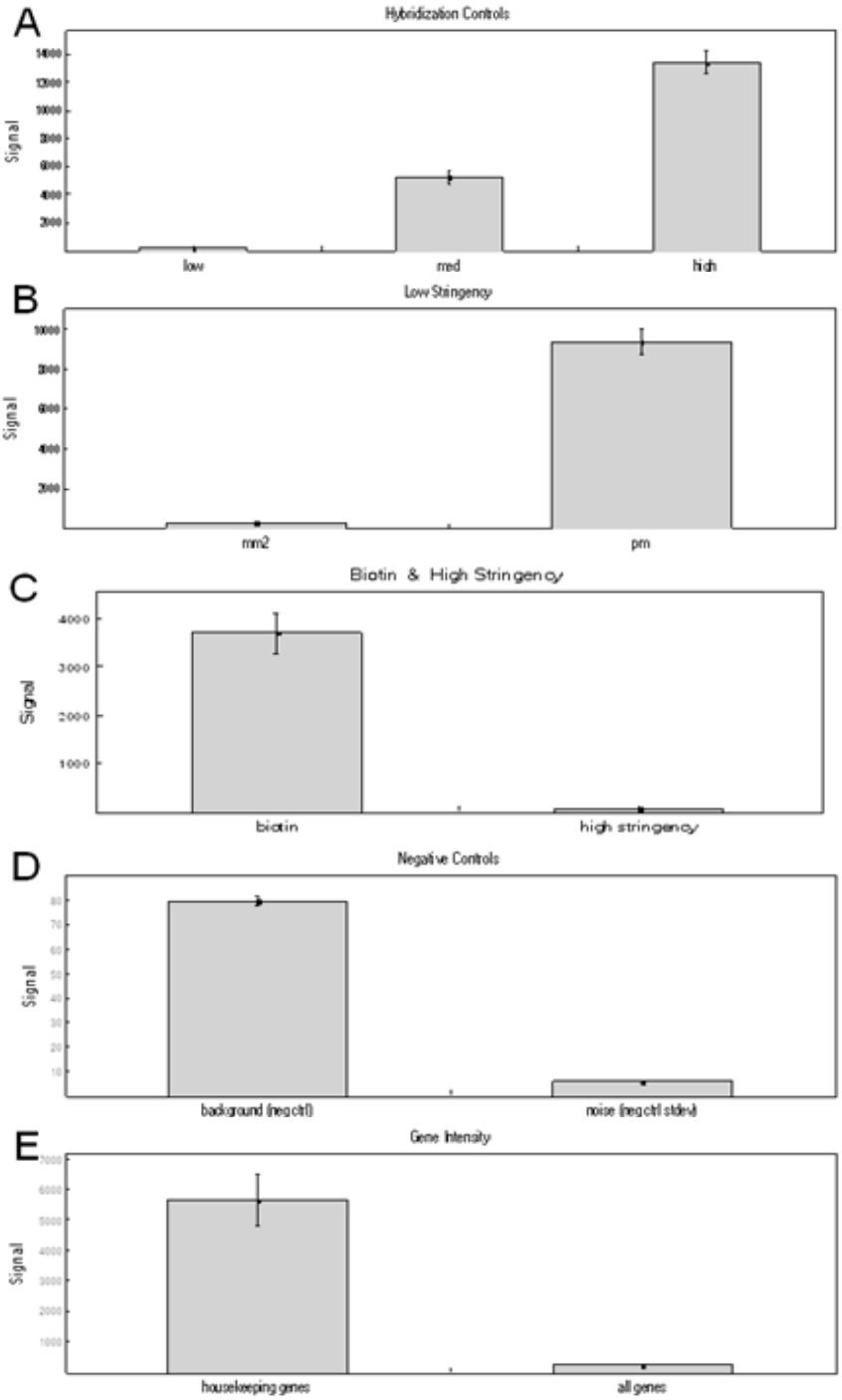

cDNA was generated from WT and Nox2$^{-/-}$ DOX-treated mouse LV (n=3) and used in evaluation of signal intensity using probes for: (A) Hybridisation; (B) Mismatch (mm2) and perfect match (pm); (C) biotin; (D) background and noise and (E) gene intensity. Signal was measured as fluorescence and expressed in arbitrary units. Bar graphs were generated by Cambridge Genomic Services.

FIGURE S4: Comparison of normalised transcript data within samples from WT and Nox2$^{-/-}$ mice.

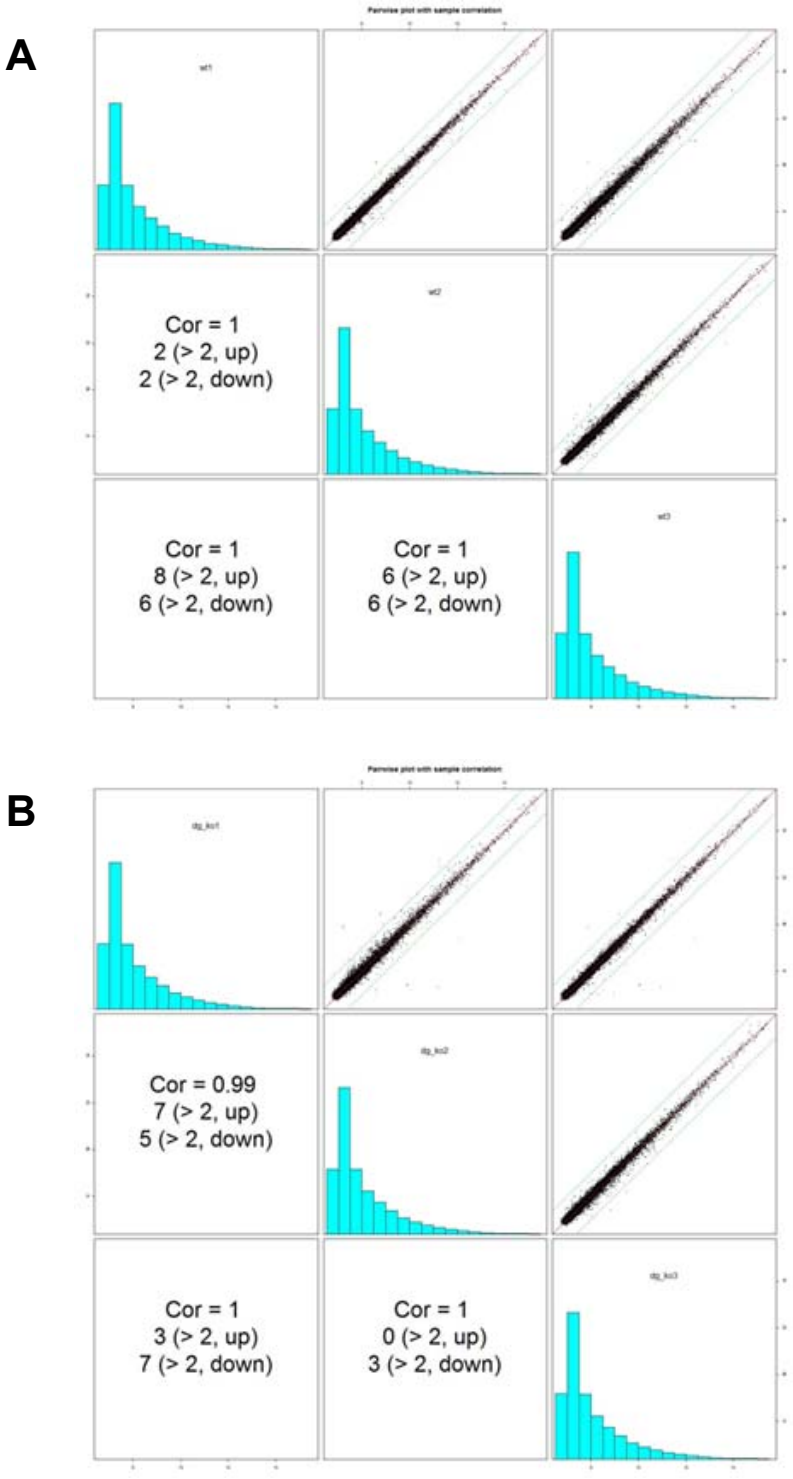

A correlation coefficient (Cor) was generated between each sample in the (A) WT group and (B) Nox2$^{-/-}$ group. Graphs were generated in the *R* programme using the *lumi* package by Cambridge Genomics Services.

FIGURE S5: Concentration responses for optimisation of experimental conditions for the ApoTox-Glo Triplex assay in HL-1 cardiomyocytes

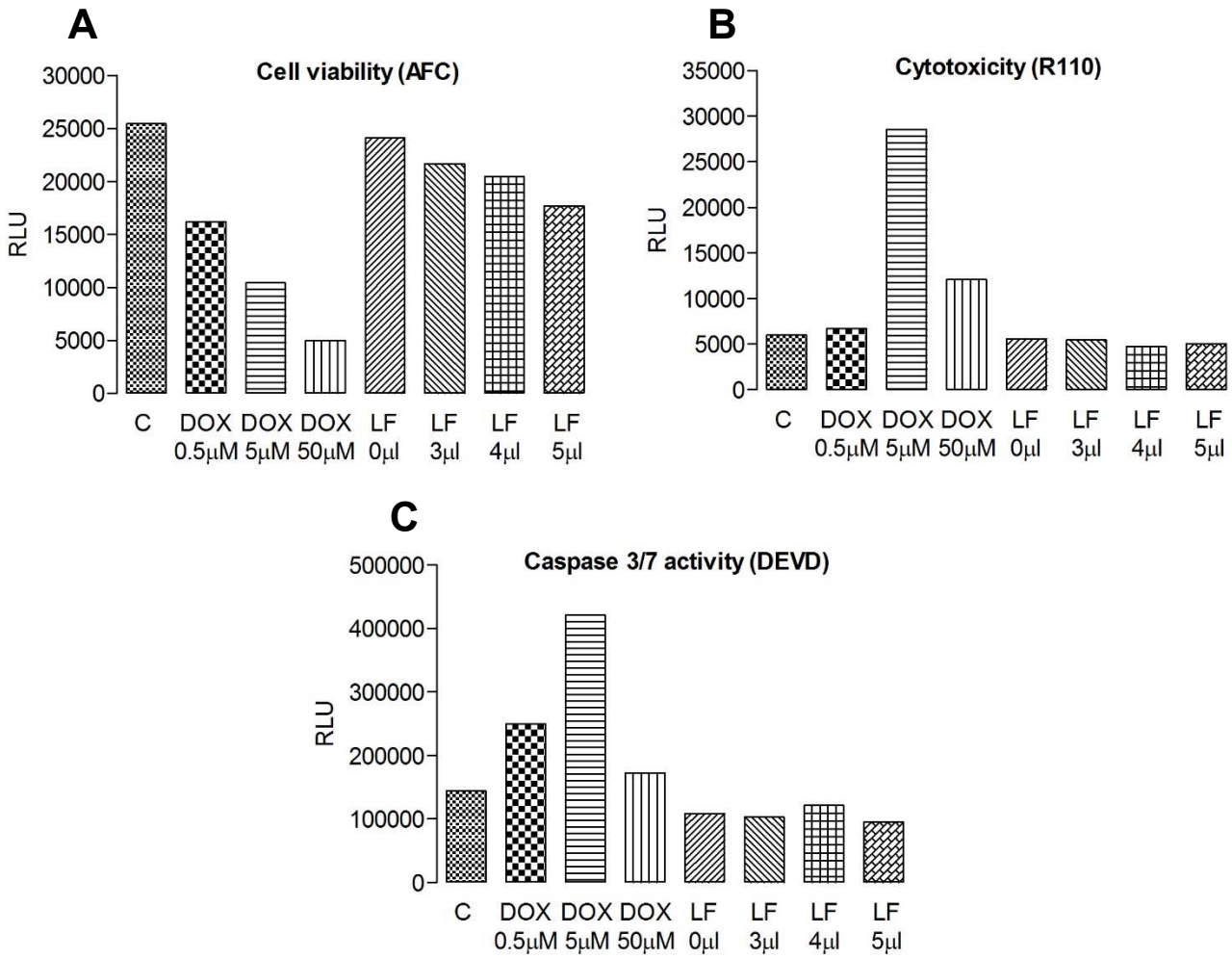

HL-1 cardiomyocytes (seeded 20000 cells/well) in a 96 well plate format were incubated in normal medium (Control, C) or with increasing concentrations of DOX (0.5µM, 5µM, 50µM), or varying volumes (0-5µl/100µl total well volume) of LF2000 (LF) for 24h prior to detection by fluorescence. (A) Cell viability (aminofluorocoumarin, AFC) and (B) cytotoxicity (rhodamine 110, R110), and by luminescence (C) Caspase 3/7 activity (cleavage of DEVD). Data are shown as average value (n=2, 8-10 replicates in each). RLU, relative light units.